U.S. Department of
Transportation

**Federal Railroad
Administration**

Passenger Cab Car Grade Crossing Impact Test Report

Rail Passenger Equipment Impact Tests

Office of Research
and Development
Washington, DC 20590

REPORT DOCUMENTATION PAGE

1. AGENCY USE ONLY (Leave blank)	2. REPORT DATE October 2007	3. REPORT TYPE AND DATES COVERED Final Report June 2002

4. TITLE AND SUBTITLE Passenger Cab Car Grade Crossing Impact Test Report	5. FUNDING NUMBERS RR28/EB035
6. AUTHOR(S) Tyrell, David; Martinez, Eloy; Jacobsen, Karina; Perlman, Benjamin	

7. PERFORMING ORGANIZATION NAME(S) AND ADDRESS(ES) U.S. Department of Transportation Research and Innovative Technology Administration John A. Volpe National Transportation Systems Center 55 Broadway Cambridge, MA 02142-1093	8. PERFORMING ORGANIZATION REPORT NUMBER DOT-VNTSC-FRA-08-01

9. SPONSORING/MONITORING AGENCY NAME(S) AND ADDRESS(ES) U.S. Department of Transportation Federal Railroad Administration Office of Research and Development 1120 Vermont Avenue, NW–Mail Stop 20 Washington, DC 20590	10. SPONSORING/MONITORING AGENCY REPORT NUMBER DOT/FRA/ORD-07/24

11. SUPPLEMENTARY NOTES

12a. DISTRIBUTION/AVAILABILITY STATEMENT This document is available to the public through the National Technical Information Service, Springfield, VA 22161. This document is also available on the FRA Web site at www.fra.dot.gov.	12b. DISTRIBUTION CODE

13. ABSTRACT (Maximum 200 words)

Two full-scale oblique grade crossing impact tests were conducted in June 2002 to compare the crashworthiness performance of alternative corner post designs on rail passenger cab cars. On June 4, 2002, a cab car fitted with an end frame built to pre-1999 requirements impacted a steel coil at approximately 14 mph (22.5 km/h). Following on June 7, 2002, a cab car fitted with an end frame built to current requirements also impacted a steel coil at approximately 14 mph (22.5 km/h).

The tests were conducted in response to a recommendation from the American Public Transportation Association's Passenger Rail Equipment Safety Standards Committee to measure the crashworthiness performance of alternative cab car end frame designs. During the test of the 1990s design, the corner post failed, eliminating the survival space for the operator. During the test of the state-of-the-art (SOA) design cab car, the corner post remained attached and deformed less than 9 in (228 mm), preserving space for the operator.

The crush of the cars was analyzed using detailed finite element models. The impact end of each car was modeled, including approximately one quarter of the length of the car. The back end of the cab car model was fixed, and its end structure was impacted by an initially moving cylinder with the same mass and dimensions as the steel coil used in the tests.

The results from the full-scale grade crossing impact tests validated the preliminary results of the three-dimensional lumped parameter computer model of the collision dynamics.

14. SUBJECT TERMS Transportation, safety, crashworthiness, passenger rail vehicles, cab car end structure, grade crossing, impact test	15. NUMBER OF PAGES 72
	16. PRICE CODE

17. SECURITY CLASSIFICATION OF REPORT Unclassified	18. SECURITY CLASSIFICATION OF THIS PAGE Unclassified	19. SECURITY CLASSIFICATION OF ABSTRACT Unclassified	20. LIMITATION OF ABSTRACT Unlimited

METRIC/ENGLISH CONVERSION FACTORS

ENGLISH TO METRIC

METRIC TO ENGLISH

LENGTH (APPROXIMATE)

1 inch (in)	= 2.5 centimeters (cm)
1 foot (ft)	= 30 centimeters (cm)
1 yard (yd)	= 0.9 meter (m)
1 mile (mi)	= 1.6 kilometers (km)

LENGTH (APPROXIMATE)

1 millimeter (mm)	= 0.04 inch (in)
1 centimeter (cm)	= 0.4 inch (in)
1 meter (m)	= 3.3 feet (ft)
1 meter (m)	= 1.1 yards (yd)
1 kilometer (km)	= 0.6 mile (mi)

AREA (APPROXIMATE)

1 square inch (sq in, in^2)	= 6.5 square centimeters (cm^2)
1 square foot (sq ft, ft^2)	= 0.09 square meter (m^2)
1 square yard (sq yd, yd^2)	= 0.8 square meter (m^2)
1 square mile (sq mi, mi^2)	= 2.6 square kilometers (km^2)
1 acre = 0.4 hectare (he)	= 4,000 square meters (m^2)

AREA (APPROXIMATE)

1 square centimeter (cm^2)	= 0.16 square inch (sq in, in^2)
1 square meter (m^2)	= 1.2 square yards (sq yd, yd^2)
1 square kilometer (km^2)	= 0.4 square mile (sq mi, mi^2)
10,000 square meters (m^2)	= 1 hectare (ha) = 2.5 acres

MASS - WEIGHT (APPROXIMATE)

1 ounce (oz)	= 28 grams (gm)
1 pound (lb)	= 0.45 kilogram (kg)
1 short ton = 2,000 pounds (lb)	= 0.9 tonne (t)

MASS - WEIGHT (APPROXIMATE)

1 gram (gm)	= 0.036 ounce (oz)
1 kilogram (kg)	= 2.2 pounds (lb)
1 tonne (t)	= 1,000 kilograms (kg)
	= 1.1 short tons

VOLUME (APPROXIMATE)

1 teaspoon (tsp)	= 5 milliliters (ml)
1 tablespoon (tbsp)	= 15 milliliters (ml)
1 fluid ounce (fl oz)	= 30 milliliters (ml)
1 cup (c)	= 0.24 liter (l)
1 pint (pt)	= 0.47 liter (l)
1 quart (qt)	= 0.96 liter (l)
1 gallon (gal)	= 3.8 liters (l)
1 cubic foot (cu ft, ft^3)	= 0.03 cubic meter (m^3)
1 cubic yard (cu yd, yd^3)	= 0.76 cubic meter (m^3)

VOLUME (APPROXIMATE)

1 milliliter (ml)	= 0.03 fluid ounce (fl oz)
1 liter (l)	= 2.1 pints (pt)
1 liter (l)	= 1.06 quarts (qt)
1 liter (l)	= 0.26 gallon (gal)
1 cubic meter (m^3)	= 36 cubic feet (cu ft, ft^3)
1 cubic meter (m^3)	= 1.3 cubic yards (cu yd, yd^3)

TEMPERATURE (EXACT)

$[(x-32)(5/9)]$ °F = y °C

TEMPERATURE (EXACT)

$[(9/5) y + 32]$ °C = x °F

QUICK INCH - CENTIMETER LENGTH CONVERSION

Inches: 0 1 2 3 4 5

Centimeters: 0 1 2 3 4 5 6 7 8 9 10 11 12 13
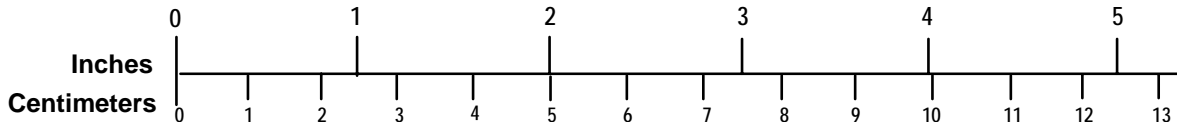
QUICK FAHRENHEIT - CELSIUS TEMPERATURE CONVERSION

°F	-40°	-22°	-4°	14°	32°	50°	68°	86°	104°	122°	140°	158°	176°	194°	212°
°C	-40°	-30°	-20°	-10°	0°	10°	20°	30°	40°	50°	60°	70°	80°	90°	100°
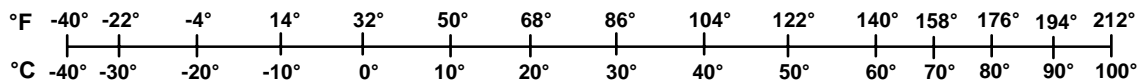
For more exact and or other conversion factors, see NIST Miscellaneous Publication 286, Units of Weights and Measures. Price $2.50 SD Catalog No. C13 10286

Preface

The grade crossing impact tests were conducted under the sponsorship of the Federal Railroad Administration's Office of Research and Development, as part of the ongoing study called the Equipment Safety Research Program. The grade crossing impact tests mark completion of the first stage of testing conventional equipment, while concurrently beginning the second stage of testing improved equipment designs.

Table of Contents

List of Figures

List of Tables

Executive Summary

Two full-scale oblique grade crossing impact tests were conducted in June 2002 to compare the crashworthiness performance of alternative corner post designs on rail passenger cab cars. On June 4, 2002, a cab car fitted with an end structure built to pre-1999 requirements impacted a steel coil at approximately 14 mph (22.5 km/h). Following on June 7, 2002, a cab car fitted with an end structure built to current requirements underwent the same test. Each car was equipped with strain gauges, string potentiometers, and accelerometers to measure the deformation of specific structural elements, as well as the longitudinal, lateral, and vertical displacements of the carbody. The gross motions of the cars and steel coil, the force-crush behavior of the end structures, and the deformation of major elements in the end structures were measured during the tests.

The tests themselves were conducted in response to a recommendation from the American Public Transportation Association's (APTA) Passenger Rail Equipment Safety Standards/Construction-Structural (PRESS C&S) Subcommittee to measure the crashworthiness performance of alternative cab car end structures. During the test of the 1990s design, the corner post failed, eliminating the survival space for the operator. During the test of the state-of-the-art (SOA) design cab car, the corner post remained attached and deformed less than 9 in (229 mm), preserving space for the operator.

Before the tests, the crush behaviors of the cars and their dynamic responses were simulated with car crush and collision dynamics (CD) models. The car crush model was used to determine the force-crush characteristics of the corner posts, as well as their modes of deformation. The CD model was used to predict the extent of crush of the corner posts as functions of impact velocity, as well as the three-dimensional accelerations, velocities, and displacements of the cars and coil. Pre-test analyses of the models were used in determining the initial test conditions, instrumentation, and locations.

The crush of the cars was analyzed using detailed finite element (FE) models. The impact end of each car was modeled, including approximately one quarter of the length of the car. The back end of the cab car model was fixed, and its end structure was impacted by an initially moving cylinder with the same mass and dimensions as the steel coil used in the tests.

Before the tests, runs were made with the models with and without material failure. This approach allowed calculation of an upper bound and a lower bound on the force-crush characteristics. The pre-test predictions of the analysis of the SOA design car, including material failure, very closely match the results of the test for the force-crush characteristic, strains at the measured locations, the geometry of the deformed structure, and the locations and extent of material failure. The pre-test predictions of the analysis of the 1990s design also closely match the test measurements; however, the extent of material failure predicted was slightly less than observed in the test. Failure of the corner

post was predicted to occur at a speed of 1.6 mph (2.57 km/h), approximately 10 percent greater than the test speed. A more sophisticated implementation of the material failure modeling helped bring the model results into very close agreement with the test measurements.

The CD was analyzed using a lumped parameter model, with nonlinear stiffness characteristics. The suspension of the car is included in the model in sufficient detail to predict derailment. The model uses the force-crush characteristic developed in the car crush analysis as input and includes the lateral force that develops as the corner post is loaded longitudinally.

The results from the full-scale grade crossing impact tests agree with and confirm the preliminary results of the three-dimensional lumped parameter computer model of the CD. The predictions of the three-dimensional accelerations, velocities, and displacements of the car and the coil are in very close agreement with the measurements made in the tests of both cars, up to the time of failure of the corner post. The cars remained on the track in both tests, as predicted with the model.

1. Background

In January 2000, the APTA Commuter Rail Chief Executive Office (CEO) Executive Committee requested the FRA Office of Research and Development to develop information on the effectiveness of APTA's recently introduced *Manual of Standards and Recommended Practices for Passenger Rail Equipment* [1] and FRA's recently established regulations [2]. APTA was particularly interested in the increase in crashworthiness associated with the additional and revised cab car end frame standards and regulations. These standards and regulations are intended to provide crashworthiness in the event of a grade crossing collision, train-to-train collision, or impact with an object fouling the right-of-way.

FRA included full-scale impact tests and associated planning and analysis activities in its overall research plans to develop the information requested. The details of the tests were developed in conjunction with the APTA/PRESS C&S Subcommittee.

FRA developed the information on cab car crashworthiness requested by APTA in four steps:
- Step 1: Design Development of Test Articles
- Step 2: Development of Test Conditions
- Step 3: Implement Tests
- Step 4: Compare Performance

These steps were carried out in close coordination with the APTA/PRESS C&S Subcommittee, as follows.

On November 1, 2000, at the Drake Hotel in Chicago, the specific objectives of the test and alternative test conditions were discussed during a meeting of a steering group formed by the APTA/PRESS C&S Subcommittee. At that meeting, the working group agreed that the corner post—the vertical structural member located where the sidewall meets the end wall—would be the focus of the tests, that the comparison would be with a cab car end structure design meeting the then-current standards and a design meeting typical practice immediately prior to the development of the standards and regulations, and that the test approach would be a cab car impacting a free-standing coil of steel. The corner post was chosen to address longstanding FRA concerns about the corner structure of cab cars. The end structure designs were chosen to address the APTA CEO's request to clarify "how much the new standards had bought them."

Alternative test approaches considered by the working group included:
1. A quasistatic large deformation test
2. A dynamic test of a car into a fixture mounted on a fixed wall
3. A dynamic test of a car into a fixture mounted on a rail car
4. A dynamic test of a car into a steel coil test article mounted on a highway flatbed-tractor trailer
5. A dynamic test of a car into a free-standing steel coil

The working group eliminated the quasistatic test approach because of the difficulty in assuring that the support conditions for the rail car structure during such a test would simulate or closely approximate the support conditions for the structure under dynamic (accident) conditions. The working group, because of the low-test speeds required to cause significant structural damage, eliminated the approach of mounting a fixture to a wall. The group eliminated the approach of mounting the test article to the flat car due to the relative complexity of the test. The group also eliminated the approach of recreating an accident because of the difficulties associated with analyzing the behavior of more than two impacting objects [3]. The complex interactions of multiple deformable bodies make it a practical impossibility to design a repeatable test. In addition, such an approach requires detailed modeling of the highway vehicle. The group agreed that resources would be better employed by further analyzing the rail car structure. The group selected the approach of the cab car impacting a freestanding coil. This approach has the advantages of being relatively simple to set up; it is repeatable with careful setup; and the impact speeds and loading conditions closely approximate accident conditions. Section 3 of this report provides an overview of the test, and Appendix B includes the detailed test requirements.

At the January 17, 2001, meeting of the APTA/PRESS C&S Subcommittee, held at APTA's headquarters in Washington, DC, the decisions of the working group were presented and discussed. The stated objective of the test was to compare the crashworthiness performance of pre- and post-1999 corner post designs for cab cars, as well as show the required loads in the then-current APTA Standards (post-1999 requirement), that the cab car end structure must withstand. A grade crossing test approach was proposed using a 40,000 lbm (18,144 kg) steel coil on a frangible support run twice: once with a cab car compliant with pre-1999 regulations and once with a cab car compliant with post-1999 regulations. An overview of the pre-1999 regulations was discussed along with the following cautions:

- The specifications prescribed the static loads that the structure must support.
- The specifications do not fully prescribe how the structure should behave under those static loads.
- The test results will likely be related to the amount of energy absorbed.
- A design compliant with pre-1999 practice may potentially have greater crashworthiness if it absorbs more energy.

Preliminary test predictions of various cab car end frame design concepts were presented according to the maximum safe speed for operators and passengers in a crash.

Overview of the designs of the cab car end frames to be tested was presented at the July 19, 2001, meeting of the C&S Subcommittee, held in Washington, DC. Examples of two designs were to be tested: a 1990s design, compliant with typical practice of the 1990s, and an SOA design, compliant with all of the FRA regulations and APTA standards then in place. These designs were developed to be retrofitted to Budd Pioneer cars. The 1990s design is characterized by a stepwell and a relatively light corner post. In contrast, the cross-section of the SOA design corner post is larger, and the side sill is continuous

4

(i.e., no stepwell exists). A recent purchase by New Jersey Transit indicated a willingness to eliminate a stepwell. In addition, modifications to the draft sill would have been required if the stepwell had been retained, while no modifications were necessary with a continuous side sill. The differences in the designs were principally driven by the then-current APTA standard requiring severe deformation of the corner and collision posts before failure of the attachments. Section 2 presents a more extensive overview of the designs, and another cab car end structure report [4] includes detailed descriptions of the designs.

A cab car with an end frame built to the 1990s design was impact tested on June 4, 2002, and a cab car with an end frame built to the SOA design was tested on June 7, 2002. Both tests were conducted at the Transportation Technology Center (TTC) in Pueblo, CO. The impact speed in both tests was approximately 14 mph (22.5 km/h). In the test of the 1990s design, the corner post failed, eliminating the operator's survival space. In the test of the SOA design, the corner post deformed by 9 in (228 mm). The corner post did not fail, thereby preserving the operator's survival space. The 1990s design has a maximum safe speed—the maximum speed for which the operator's space will be preserved—of 11 mph (17.7 km/h). The SOA design has a maximum safe speed of 16 mph (25.7 km/h), an increase of nearly 50 percent. Sections 3 and 4 present a more extensive overview of the test results, and Appendix A includes detailed descriptions of the results.

Preliminary results of these tests were presented at the APTA/PRESS C&S Subcommittee Meeting held October 29, 2002, at Southeastern Pennsylvania Transportation Authority (SEPTA) in Philadelphia, PA. Detailed results were presented at the APTA/PRESS C&S Subcommittee Meeting, March 4, 2003, held in Washington, DC. An overview of the development of the 1990s and SOA designs, development of the test conditions, implementation of the tests, and the test results were presented at the APTA/PRESS Committee Meeting, May 22, 2003, Newark, NJ. Two technical papers on the preliminary results of these tests were presented and published in April 2003 [5][6].

In spite of the results of the effort, which showed a significant increase in crashworthiness resulting from the then-current APTA standards, the APTA/PRESS Committee voted to accept significant changes to their standards for cab car end structures. The standards requiring that the corner and collision post sustain severe deformation before failure of the post attachments were replaced with a recommended practice that these attachments be able to sustain minimum prescribed loads with negligible deformation.

2. Introduction

The goals of this crashworthiness research program are to provide a survivable volume for the operator to safely ride out the collision and to minimize the forces imparted to the operator during the ride down phase of the collision. The safe allowable crush distance for the end frame is defined as 12 in (305 mm). Any crush in excess of this distance may result in the bulk crushing of the operator.

Several collisions have occurred in recent accident history during which the end frame structure was engaged above the underframe and a subsequent loss of operator survivable volume occurred. Two recent examples of such collisions include the Yardley, PA, collision between a cab car-led commuter train and a tractor semitrailer carrying coils of steel [7] and the Portage, IN, grade crossing collisions between a cab car-led commuter train and a tractor-tandem trailer carrying coils of steel [8].

Figure 1 is a series of photographs taken from the collision that occurred in Portage, IN, on June 18, 1998, where a cab car-led passenger train collided with the flatbed loaded with steel coils of a semitrailer stuck at a grade crossing. When the train impacted the flatbed, one of the restraining straps snapped, causing a 40,000 lbm (18,100 kg) steel coil to penetrate the bulkhead and collision post and proceed to roll through the passenger compartment. This collision resulted in five minor injuries and three fatalities. The left picture is the impacted end of the lead cab car, the middle is an interior shot of the broken collision post, and the right is the steel coil after the accident.

Figure 1. Post-Accident Photographs of Portage, IN, Grade Crossing Collision

The purpose of such testing is to establish the minimum level of crashworthiness enhancement by modifying current designs using increased strength-based requirements. The motivation for such testing comes about as a result of the danger posed to operators of cab cars when operating a consist in the push mode. Under these operational conditions little space exists between the operator and any object that the cab car may strike during a grade crossing collision or a collision with an obstruction fouling the right-of-way of the consist.

3. Overview of Cab Car End Structures

The purpose of the end frame structure is to provide protection for the operator and passengers of a cab car in the event of a collision with the superstructure of the vehicle. This structure is composed of several structural elements that act together to protect the occupants. The base of the end frame structure is composed of the end/buffer beam, which is directly connected to the draft sill of the vehicle. For cars that include stepwells, the side sills of the underframe generally do not directly connect to the end/buffer beam. Four major vertical members are connected to the end/buffer beam: two collision posts located at roughly one-third points along the length of the end/buffer beam and two corner posts located at the outermost width of the vehicle. These structural elements are also connected together through two additional lateral members, a lateral member/shelf located just below the window frame structure and at the top by an anti-telescoping (AT) plate. The attachment of the end frame structure typically occurs at three locations to the rest of the vehicle. The first location is at the draft sill at the level of the underframe. This is the main connection where a majority of any longitudinal load applied to the end frame is transferred into the underframe of the vehicle. Two other connections at the cant/roof rail are located at either side of the car just below the level of the roof. When a longitudinal load is applied to the end frame, it is reacted by the draft sill and the cant rails into the main carbody structure. Figure 2 depicts a schematic of a typical arrangement.
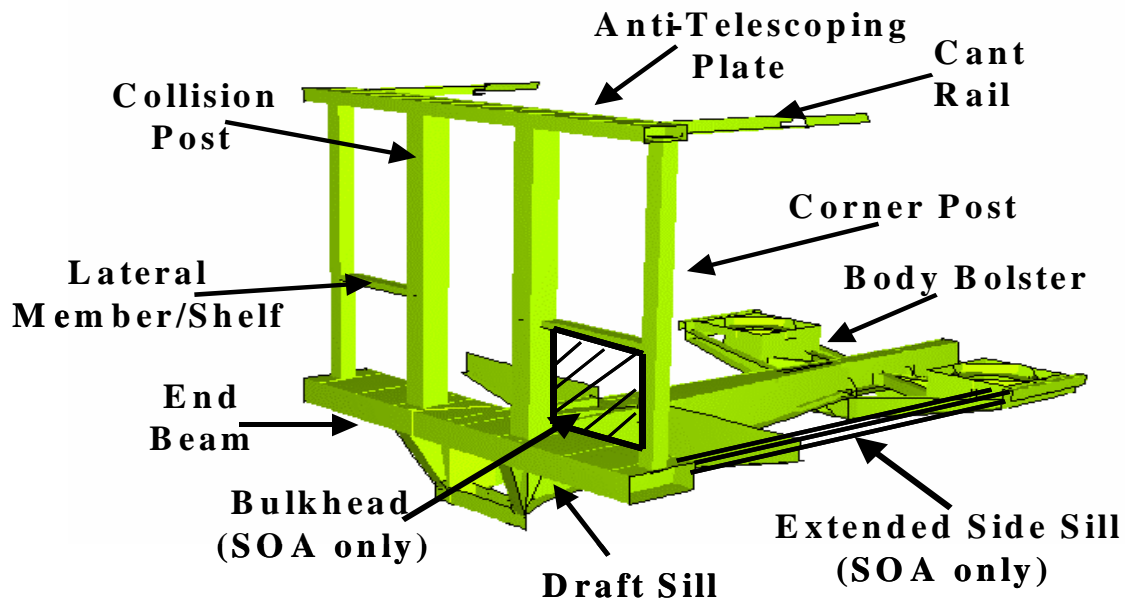

Figure 2. Schematic of Key Structural Components of the Cab Car End Frame Designs

3.1. Cab Car End Frame Designs

Two end frame designs were developed for the grade crossing testing program. The first end frame design is representative of typical designs of passenger rail vehicles before 1999. The second end frame design incorporated all the enhanced requirements passed in 1999 from the Federal regulations in 49 CFR Parts 238 and APTA SS-C&S-034-99 Standard for the Design and Construction of Passenger Railroad Rolling Stock. The second end frame design is referred to as the SOA design. The two end frame designs developed were then retrofitted onto two Budd Pioneer passenger rail cars for testing.

Two Budd Pioneer cars [9] were modified with the end frame designs. The draft sill, body bolster, and cant rail from the Pioneer car were retained, while the AT plate, end beam, collision posts, corner posts, and lateral member/shelf were replaced with updated designs. Many of the elements are similar for the 1990s and the SOA designs, including the end/buffer beams and AT plates.

The principal differences between the two designs are the size of the corner posts, the presence of a bulkhead sheet attached from the lateral member/shelf to the collision post to the corner post and to the end beam on the SOA design, and the length of the side sill on the SOA design which extends past the rear operator compartment to the end beam removing the presence of the stepwell. Figure 3 and Figure 4 show the design comparisons. In addition to changes in the cross-sectional sizes and thickness of some structural members, another change is associated with the connection details for the corner posts. The collision posts of both designs penetrate the top and bottom flanges of the end/buffer beam and the AT plate. This is based upon typical practice in the early 1990s for the 1990s design and a requirement in the APTA standard for the SOA design. The corner posts differ, because the corner posts for the 1990s design do not penetrate both top and bottom flanges of the end/buffer and AT beams while the posts of the SOA design do. The SOA design therefore has a significantly stiffer connection that is better able to resist torsional loads transferred to the AT plate.
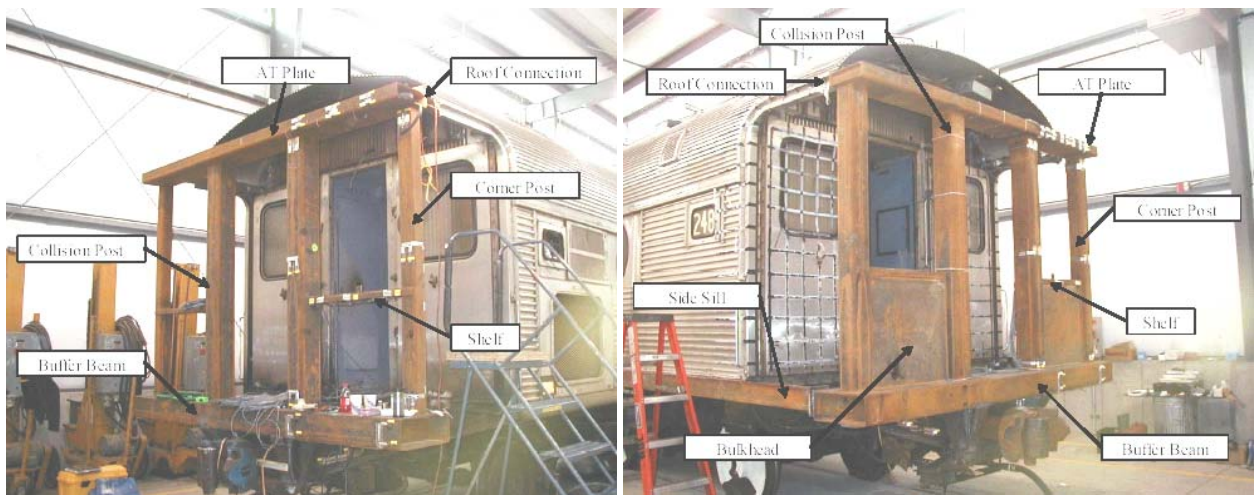
Figure 3. Photographs of 1990s (Left) and SOA (Right) End Frames

1990s Design

0.25-in lug

0.375 in

7.75 in

6.5 in

Collision

0.25 in   0.25-in lug

4.5 in

4.5 in

Corner

SOA Design

0.375-in lug

0.375 in

7.75 in

6.5 in

Collision

0.3125 in   0.3125-in lug

6 in

6 in
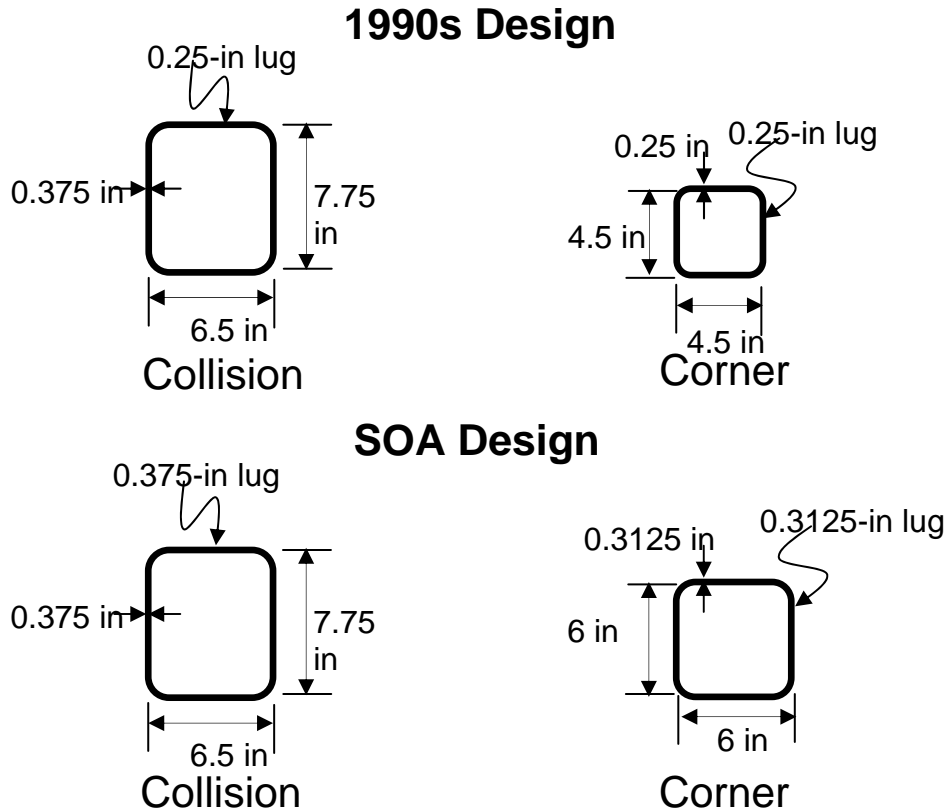
Corner

Figure 4. Schematics Contrasting 1990s and SOA End Frame Designs; Collision and Corner Posts as Tested

Both end frame designs were constructed primarily with A710 steel. A710 is becoming popular for use in the rail industry because of the higher nominal material properties and the increased ductility. Such properties allow for construction of individual structural elements of smaller cross-section and thinner thickness. Higher ductility and thinner thicknesses increase the permanent deformation that a structure can sustain before material failure starts to occur.

3.2. Overview of 1990s and SOA End Frame Design Requirements

As part of the development of the two end frame designs, a survey of existing cab car end frame designs was conducted, and detailed design requirements were developed for each design. The survey helped define the range of cross-sectional geometries for the end frame members and the approaches used in connecting these members. The design requirements describe in detail the functions and constraints of the designs, including the geometric (space) requirements, the service load requirements, the collision load requirements, and the fabrications requirements. Appendix A includes a more detailed overview of the design requirements and the evolution of the collision requirements. The results of the survey and all of the design requirements for both end frame designs are described in reference [4].

The design requirements for the 1990s end frame design are based upon the strength requirements from the industry standard, as well as typical industry practice. The

Association of American Railroads (AAR) discontinued maintenance of the AAR S-034 in 1983. Subsequently, APTA developed an enhanced version of the standard and released a revised standard entitled, "APTA SS-C&S-034-99 Standard for the Design and Construction of Passenger Railroad Rolling Stock," in 1999. The SOA end frame design developed for this testing program included all requirements listed in the 1999 APTA standard, as well as those required by 49 CFR Part 238 regulations, also passed in 1999. Differences in the requirements for the 1990s design and the SOA design were higher values for the static load requirements for key end frame members, as well as a requirement on the performance of the collision and corner posts when overloaded. The 1999 APTA requirements for cab car end structures included the following statement:

> ….post and its supporting structure shall be designed so that when it is overloaded … failure shall begin as bending or buckling in the post. The connections of the post to the supporting structure, and the supporting car body structure, shall support the post up to its ultimate capacity. The ultimate shear and tensile strength of the connecting fasteners or welds shall be sufficient to resist the forces causing the deformation, so that shear and tensile failure of the fasteners or welds shall not occur, even with severe deformation of the post and its connecting and supporting structural elements.

The term severe deformation is ambiguous, but after discussions with APTA technical staff, the severe deformation requirement was defined as a horizontal crush of the post a distance equal to its depth. Some failure of the parent material was allowed in the post but no failure was allowed in the welded connections.

An additional difference in the requirements was the exclusion of the stepwells to allow for extended side sills from the body bolster to the end/buffer beam. Recent car orders—notably the New Jersey Arrow 7 procurement—allowed elimination of the stepwells on the car end of the car. By bringing the side sills forward to support the end/buffer beam directly at the corners, the size of the end/buffer beam could be maintained to a similar size as the one developed for the 1990s design.

Table 1 shows a summary of the design requirements developed for both the 1990s and the SOA end frame designs.

Table 1. Summary of Cab Car End Structure Crashworthiness Standards and Requirements

Component	Standard/Requirement	
	1990s Design	SOA Design
Collision Post (must be present at the 1/3 points along the width of the vehicle)	• 300x10^3 lbf (1,334 kN) at the floor without exceeding the ultimate shear strength • 300x10^3 lbf (1,334 kN) at 18 in (457 mm) above the floor without exceeding the ultimate strength • Both requirements apply for loads applied ±15 degrees inward from the longitudinal • If reinforcement is used to achieve the strength, it must extend fully to 18 in (457 mm) and then taper to 30 in (762 mm) above the underframe	• 500x10^3 lbf (2,224 kN) at the floor without exceeding the ultimate shear strength • 200x10^3 lbf (890 kN) at 30 in (762 mm) without exceeding the ultimate strength • 60x10^3 lbf (267 kN) applied anywhere without yield • All requirements apply for loads applied ±15 degrees inward from the longitudinal • Strengths must be achieved without failing connections • The post must be able to deform substantially without failing the connections
Corner Post (must be present at the extreme corners of the vehicle)	• 150x10^3 lbf (667 kN) at the floor without exceeding the ultimate shear strength • 30x10^3 lbf (134 kN) at 18 in (457 mm) above the floor without exceeding the material yield strength • Both requirements apply for loads applied anywhere between longitudinal to transverse inward	• 300x10^3 lbf (1,334 kN) at the floor without exceeding the ultimate shear strength • 100x10^3 lbf (445 kN) at 18 in (460 mm) above the floor without exceeding the yield strength • 45x10^3 lbf (200 kN) applied anywhere along the post without yield • All requirements apply for loads applied anywhere between longitudinal inward to transverse inward
Lateral Member (must be present between the corner and collision posts just below the cab window)	• 15x10^3 lbf (66.7 kN) applied in the longitudinal direction anywhere between the corner and collision post without yield	• 15x10^3 lbf (66.7 kN) applied in the longitudinal direction anywhere between the corner and collision post without yield • Include a bulkhead in the opening below the shelf

The FRA regulation and APTA standards do not fully prescribe all the requirements that a functional cab car end structure must meet; that is, they are necessary but not sufficient to fully describe the design. Many alternative designs can potentially meet the regulations and standards, and each may be expected to behave somewhat differently under dynamic loading conditions. In addition to the static loads prescribed by FRA regulations and APTA standards, the SOA design was also developed against requirements for post-yield behavior (i.e., the structure was designed to deform gracefully). A draft report that is currently being reviewed for publication describes the full set of design requirements, the static load tests performed to demonstrate compliance of the designs to the appropriate regulations and standards, and the details of the designs themselves.

3.3. Evaluation of Severe Deformation

Figure 5 shows representative results from a large deformation quasistatic analysis of the corner post subjected to an overload. The load is applied at a height of 18 in (457 mm) above the corner post to the end/buffer beam connection. The load is supported by the corner post and the following support members: the lateral shelf, the bulkhead sheet, the corner post-cant rail-AT plate connection, and the corner post-end/buffer beam-extended side sill connection. The lateral shelf and the bulkhead sheet are very effective in shedding load into the rest of the end frame structure. A plastic hinge has formed at the corner post-end/buffer beam-extended side sill connection. The corner post-cant rail-AT plate connection experienced torsional deformations. These deformations result in plastic hinges forming at both the cant rail-AT plate connection and the connection of the collision post to the AT plate.
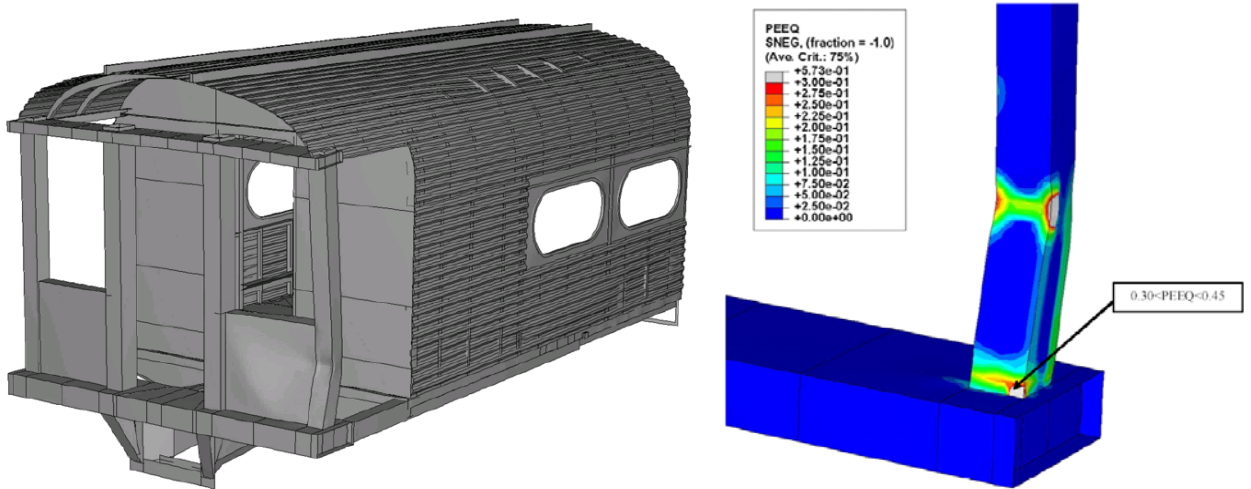

Figure 5. Corner Post Mode of Deformation at 7.75 in (197 mm) of Crush; Load Applied 18 in (457 mm) Above Floor

The contour plot of effective plastic strain for the corner post shows some areas of the post exhibiting strains in excess of the elongation strain on the material certification sheets for the A710 plate stock used to construct the corner post. The bulkhead sheet has been removed for clarity. The deformation state shown is for the corner post at 7.75 in (197 mm) of inward longitudinal deformation. The areas where the strains are highest are where failure of the post would be expected.

Figure 6 shows a plot of the force-deflection characteristic of the SOA end frame under this loading condition. The shape of the curve has an initial linear portion of the curve associated with the linear elastic behavior of the post; then once the peak load is reached at approximately 235,000 lbf (517,000 kg), the curve plateaus over the next 6 in (152 mm). The fact that no failure is included in the model results in the force plateau continuing out past 12 in (305 mm) of crush. The actual characteristic would instead reach a peak value and then gradually drop off until failure at the base of the post. At that point the load would drop off significantly. From the contour plot of effective plastic strain shown in Figure 5, the results after 7.75 in (197 mm) of inward deformation become questionable. Up to a crush distance equal to the depth of the corner post,

however, no excessive strains are predicted, and the corner post is compliant with the severe deformation requirement.
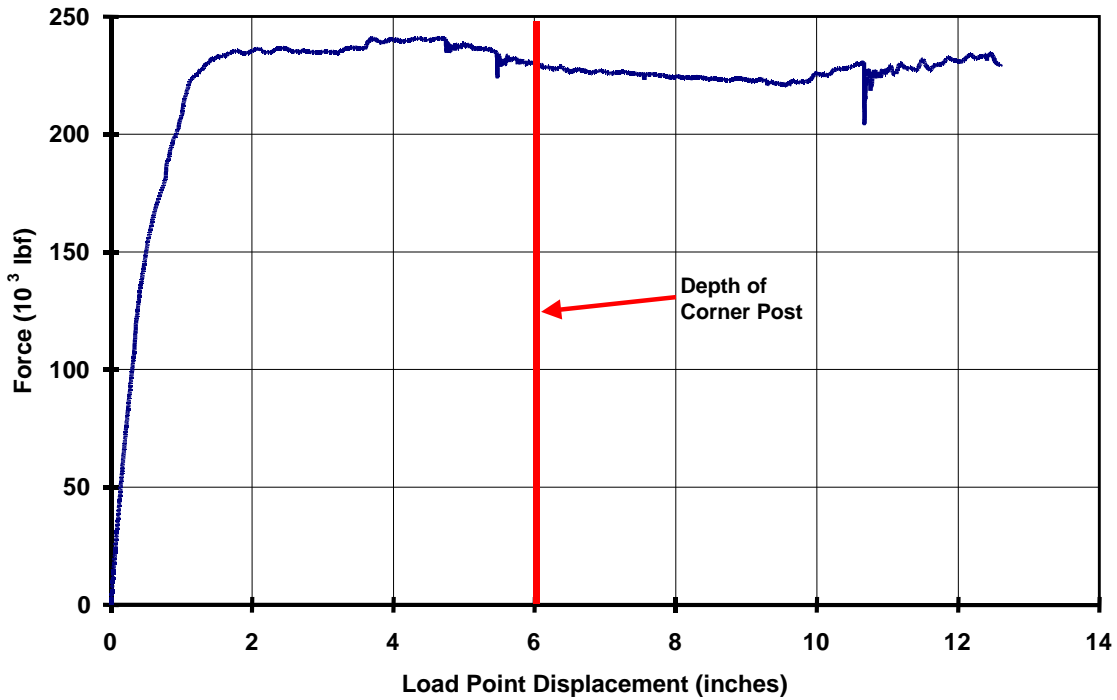
Figure 6. Force on the Corner Post Structure Over the Crush Distance

Current Federal regulations and the 1999 APTA standards for passenger car end frames prescribe minimum static loads that the structure must support without failure. While static loads prescribe minimum levels of strength requirements, such specifications do not fully account for the structural behavior of an end frame under dynamic conditions. In a dynamic test, the crush of the end frame can be characterized in terms of energy absorbed over the distance crushed. An end frame with posts that can deform significantly before failing will absorb more energy. A design consistent with pre-1999 practice may potentially provide greater crashworthiness protection if it absorbs more energy than a design compliant with the current Federal regulations and the 1999 APTA standard.

4. Test Conditions

Figure 7 is a schematic of the grade crossing test. The two full-scale tests conducted involve modified Budd Pioneer cab cars impacting a steel coil supported on a frangible table. The coil, weighing approximately 40,000 lbm (88,000 kg), was positioned with the bottom of the coil just above the height of the cab car floor and centered on the corner post in plain view. The test's objective was to measure the effectiveness of the corner post in preserving the occupant volume. Examples of such a collision scenario are discussed earlier and include the Yardley, PA [7], collision and the Portage, IN [8], collision involving steel coils penetrating the end structure of cab car-led passenger trains.

Two different end frames were tested, one typical of practice in the 1990s and one compliant with current FRA regulations and APTA recommended practices. In both tests, the coil was impacted at approximately 14 mph (22.5 km/h). This speed was chosen so that excessive intrusion (more than 12 in or 305 mm) into the operator's survival volume would occur in the test of the 1990s design and limited intrusion (less than 12 in or 305 mm) in the test of the SOA design.
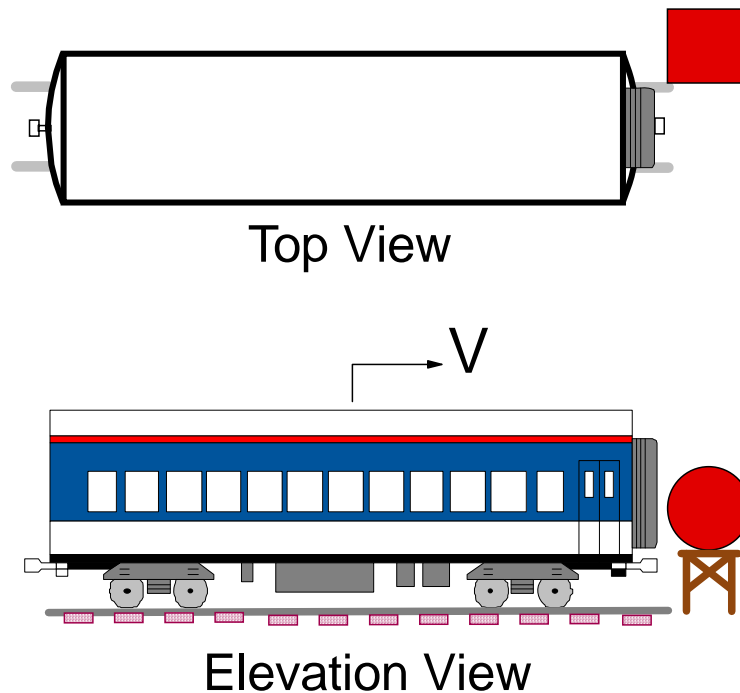
Figure 7. Schematic of In-Line Collision Scenario

Figure 8 shows a photograph of the test setup for the 1990s design. The car was instrumented to measure the accelerations of the carbody, the displacements of the suspensions, the displacements of the corner posts, and the strains in selected structural members. The coil was instrumented to measure its three-dimensional acceleration,

including yaw, pitch, and roll. Onboard and wayside high-speed film and video cameras were used to record the impact. Appendix B details the instrumentation and test requirements. The same instrumentation setup was used in the test of the SOA design. In both tests, a locomotive was used to push the cab car up to speed; the cab car was then released and impacted the coil.

Figure 8. Setup of 1990s Design Test

5. Comparison of Crashworthiness

During the full-scale test, the force on the 1990s end frame exceeded the corner post's predicted failure point, and the corner post separated from its upper attachment. Upon impact, the corner post began to hinge near the contact point with the coil; tearing at the upper connection subsequently occurred. The intensity of the impact ultimately caused the upper connection of the corner post and AT plate to fail. More than 30 in (762 mm) of deformation occurred. The SOA design performed very closely to pre-test predictions made by the FE and CD models. The SOA design crushed approximately 9 in (229 mm) in the longitudinal direction. Figure 9 shows post-collision photographs.

Figure 9. Photographs Comparing the Corner Post Crush of the 1990s (Left) and SOA (Right) End Frame Designs

In planning the grade crossing test, extensive pre- and post-test analyses were conducted to determine the impact speed and the measurement requirements; Appendix A describes the results of these analyses in detail. The results from these analyses allowed for the design of the tests such that the operator's survival space was substantially reduced for the 1990s design cab car and preserved for the SOA design cab car.

Figure 10 shows a plot of the cab car maximum crush as a function of the impact speed. The black horizontal line indicates the crush at which intrusion into the occupant compartment occurs. These analyses results were used in developing the test requirements, to determine the desired impact speed of 15 mph (24.1 km/h). A single

collision speed was chosen in order to cause significant deformation of the corner post during the tests, with the expectation that the operator's survival volume would be preserved in the test of the SOA design, i.e., that the intrusion into the occupant volume would be less than 12 in (305 mm). For the test of the 1990s design, the deformation of the corner post was expected to exceed 12 in (305 mm) and consequently intrude into the operator's survival volume. Before the tests, the 1990s design corner post was predicted to fail for an impact speed greater than 16 mph (25.7 km/h). During its test, the corner post of the 1990s design cab car end structure failed at the tested impact speed of 14.4 mph (23.2 km/h), a speed approximately 10 percent slower than predicted. The graph in Figure 10 shows that the increased standards for the corner posts prove more effective in crashworthiness protection.
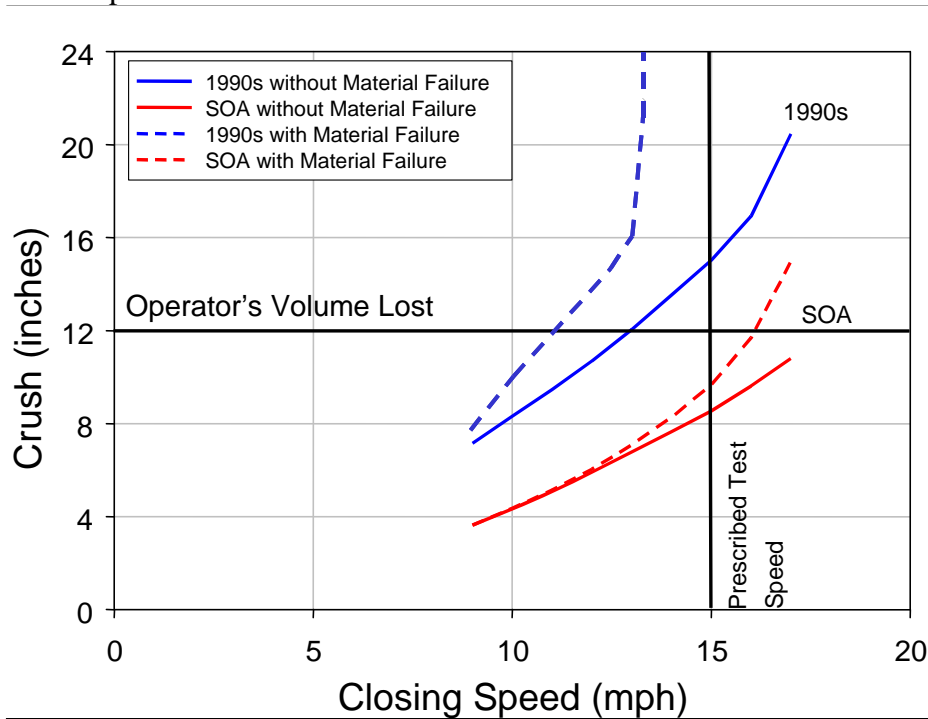
Figure 10. Comparison of Crush Estimation versus Initial Collision Speed

The above plot shows the increased level of crashworthiness performance of the SOA design over the 1990s design. Post-test results demonstrate that the 1990s design will fail at a closing speed about 5 mph (8.05 km/h) less than the SOA design. APTA's improved design standards for corner posts allow an increased ability for preserving the operator's survival volume.

6. Discussion

The grade crossing collision tests were conducted to measure the effectiveness of alternative cab car end structures in preventing intrusion during a grade crossing collision. The test conditions developed were based in part on the Portage, IN, collision [8] between a cab car-led commuter train and a tractor-tandem trailer carrying steel coils, and the Yardley, PA, collision [7] between a cab car-led commuter train with a semitrailer carrying steel coils. The results of the test of the 1990s design show that this corner post is not sufficient to preserve the operator's survival volume in such an impact. During the SOA test, the corner post remained attached, and intrusion was kept below 12 in (305 mm) of crush, thus preserving occupied volume for the conductor to ride out the collision.

The pre-test analyses are close (within 10 percent for key variables) to the test measurements taken from the 1990s end frame design test. Revision of the model to include late changes in the design and minor changes to the material failure modeling bring the model results into very close (within 5 percent) agreement with the test predictions. The pre-test analysis predictions nearly overlay the test results for the force-crush characteristic for the SOA design. Both sets of analyses are capable of predicting the correct modes of deformation and the total amount of energy consumed during the collision well. Careful application of FE modeling allowed accurate prediction of the crush behavior of rail car structures.

The 1990s end frame design was developed using practices typical of that time period. While severe deformation was qualitatively considered in developing the design, it was not quantitatively considered; the negligible deformation requirements were evaluated quantitatively to develop this design. The SOA end frame design was developed to comply with APTA's then-current severe deformation requirement. Nonlinear quasistatic FE analyses were performed to demonstrate compliance with these requirements.

The methodologies used to design the cab car end frames and the results of the tests show that significant increases in rail passenger equipment crashworthiness can be achieved if the deformation of the structure when overloaded is taken into consideration. Modern analyses methods can accurately predict the structural crush (severe deformation) and consequently can be used with confidence to develop structures that collapse gracefully. Modern testing techniques allow the verification of the crush behavior of such structures.

Appendix A.
Summary of Pre- and Post-Test Analyses Results

A.1. General Approach

The general approach used to study the crashworthiness performance of alternative designs and compare the results against conventional equipment follows several interrelated steps (see Figure A-1). An FE model is used to estimate the structural modes of deformation of the impacting bodies, as well as the areas where failure is expected to initiate and propagate. The forces absorbed by the impacting bodies are proportional to longitudinal deformation. These force-crush characteristics are then used as input into a CD model. The CD model predicts the relative displacements, the gross motions, and the secondary impact environment. The interior occupant models use the secondary impact environment information to predict the kinematics of occupants as they ride down the event and are used to predict the likelihood of injury or fatality. The results from the three models are used to design the initial and boundary conditions for the full-scale tests. They are also used to determine the types of instrumentation to be used, as well as the placements and range. The fidelity of the models is established by comparison against the full-scale test results.
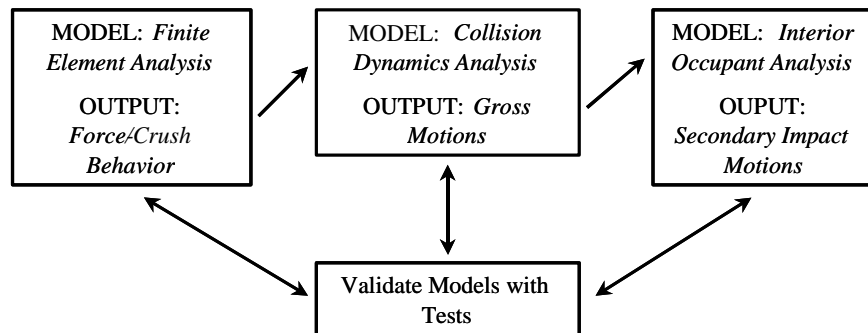
Figure A-1. Modeling Process Flowchart

In preparation for the full-scale grade crossing tests, a subset of the analyses was conducted to determine the conditions of the test, including the impact speed, and to determine the quantities to be measured. The tests were analyzed in two steps:

- Step 1: Car Crush Behavior. Detailed dynamic, nonlinear, large displacement FE models of the 1990s and SOA cab car structures were developed. An approximation to the loading condition in the test was used in these models. The principal purpose of these models was to develop the force-crush behaviors and the modes of deformation for the cab car designs. These models have been implemented in ABAQUS/Explicit [10], and all include the influence of material failure.
- Step 2: Train Collision Dynamics. Three-dimensional lumped-mass CD models were used to determine the trajectories of the cab car and coil. Impact elements

were used in these CD models, with the parameters for these elements taken from the results of the FE analyses of car crush behavior. The CD models were used to evaluate the extent of crush as a function of impact speed. These models have been implemented in ADAMS [11].

A.2. Structural Modeling and Analysis

Crush Model

Figure A-2 shows the FE model of the 1990s design integrated onto an existing cab car. The first 20 ft (6.1 m) of the car are modeled. For most of the model, the characteristic element length is about 3 in (76.2 mm). For the corner post and the area around its attachments, the characteristic element length is typically less than 0.5 in (12.7 mm) and in some cases less than 0.25 in (6.4 mm). In the model, the translations of the rear-most elements of the cab car are fixed. The rigid coil is initially given a longitudinal velocity and is then free to translate and rotate during the simulated impact. In order to bound the range of response, the model was run with and without material failure. The FE car crush model for the SOA design is similar to the model of the 1990s design.
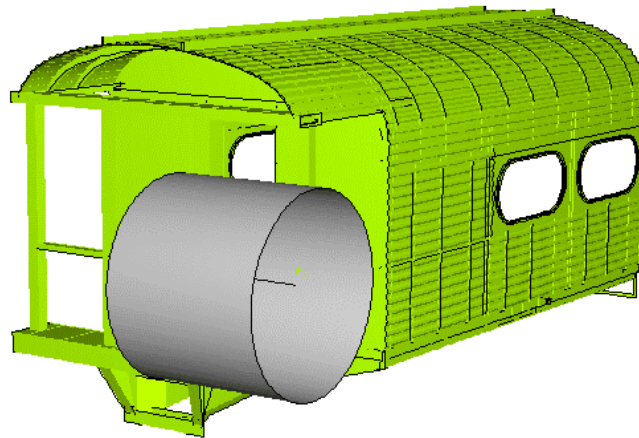

Figure A-2. FE Car Crush Model, 1990s Design

The following sections provide a detailed description of the results predicted before conducting the tests in order to develop the instrumentation requirements. Test measurements are contrasted to the pre-test predictions. The 1990s design crush model was modified after the tests were conducted to capture a failure mode not predicted beforehand but observed at the test, and these results are compared against the test measurements.

Circa 1990s Design

Figure A-3 shows the force-crush characteristic developed for the 1990s design as predicted with the model and as measured during the test. The plot shows pre-test and post-test predictions. The pre-test predictions from the analysis, including material failure and the test measurements, are in close agreement up to approximately 12 in (305 mm) of crush. After 12 in (305 mm) of crush, the pre-test predictions show the force

increasing, while the test measurements show the force decreasing. A source of the discrepancy could have resulted from late changes in the attachment of the AT plate to the cant rail that were not incorporated in the model before the test and from limitations of the current approach to modeling material failure in FE solvers. As a result, failure of the upper attachment of the corner post occurred sooner in the test than predicted.
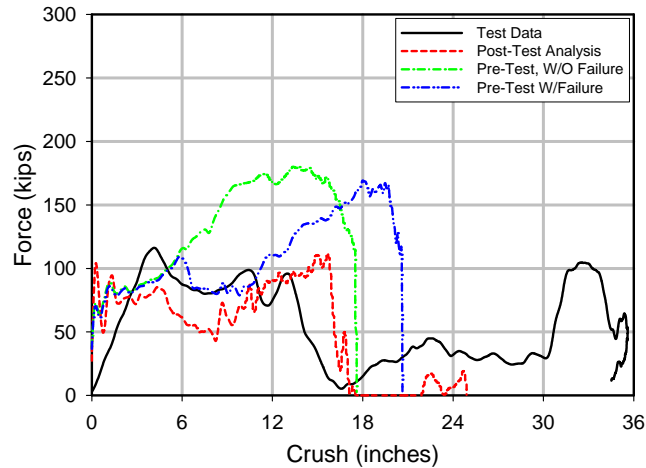

Figure A-3. Measured and Predicted Force-Crush Characteristic, 1990s Design

Instead of attaching the AT plate to the cant rails with several short gussets, as initially designed, doublers were used over the cant rails up to the bulkhead wall. In addition, several gussets were used where the doublers met the bulkhead wall. The model was revised after the test to include these changes. These changes increased the stiffness of the AT plate support, which in turn increased the stiffness of the upper attachment of the corner post.

Figure A-4 shows the force time post-test FE results, as well as the derived force time curve, taken from test measurements. A nine-accelerometer array was used on the steel coil for the test, and the force presented is the resolved acceleration times the mass of the steel coil. The results from the simulation and those derived from the test are very close for the first 0.03 second (s). Between 0.03 s and 0.05 s the measurements show somewhat elevated force levels compared to the analysis (approximately 25 percent). The results overlay one another again between 0.05 s and 0.06 s. The key difference occurs after 0.06 s where the measurements indicate softening behavior due to the failure of the lateral member/shelf and pull out of the corner post from the AT plate over approximately 0.015 s. The model is predicting a peeling/tearing failure of the lateral member/shelf from the corner post, thereby losing a source of load transfer. This resulted in a decreased load in the FE results between 0.02 s and 0.05 s. The pull out failure of the corner post from the AT plate occurs in the FE model around 0.1 s. The softening behavior occurs over a much shorter time frame at approximately 0.004 s. The differences in predicted failure response in time is not surprising given the current SOA in ductile material failure modeling.

25
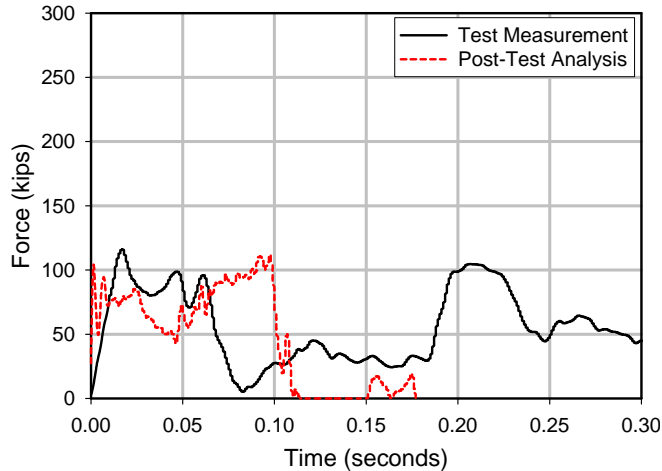
Figure A-4. Measured and Predicted Force-Time History, 1990s Design

Currently, material failure is modeled in many FE analysis packages using a simple strain-to-failure criterion. When the total strain on an element reaches a prescribed value, that element is removed from the mesh. This approach works well when the principal cause of material failure is tension and the extent of material failure is limited. An additional concern in modeling failure using this approach is the dependence of predicted strain and hence failure with mesh size. The finer the mesh, the greater the accuracy in capturing higher strain gradients and higher strain levels. The post-test model used a much finer mesh than the original model, and the failure criterion was adjusted based upon the stress state and mode of failure. A lower strain-to-failure criterion was used in the area where the corner post pulled out of the AT plate. The combination of the finer mesh and lower strain-to-failure criterion coupled with the stiffer connection caused the post-test model to fail in a manner similar to what was observed in the test. A small discrepancy exists in the results; the test measurements show pull out occurring sooner and lasting longer than what is predicted in the post-test simulation.

Figure A-5 shows a comparison of the post-test FE results taken from corresponding positions on the corner post and the measured longitudinal displacements taken from selected string potentiometers. String potentiometer position varies from bottom to top, starting at position 1 and ending at position 5 with the lead letter differentiating the test measurement (T) from the analysis result (A). The string potentiometers are symmetrically placed to equally divide the corner post between the end beam and the AT plate.
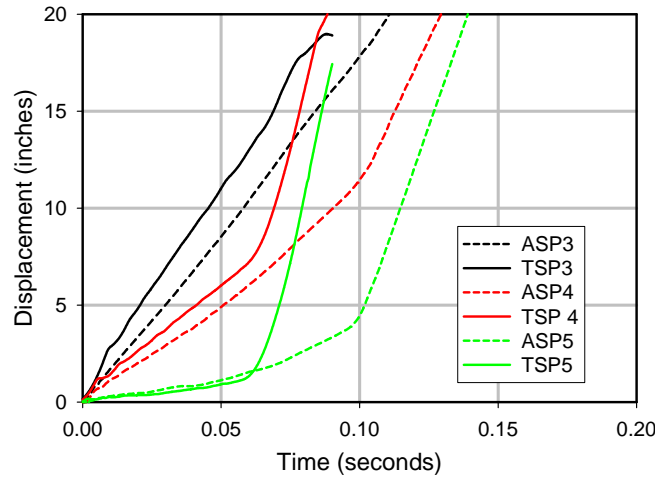
**Figure A-5. Measured and Predicted Longitudinal Displacement-Time Histories on
the 1990s Design Corner Post**

A detailed discussion of the information presented by TSP3 is given that represents the
mechanisms occurring for all the string potentiometers. The first slope occurs between
initial impact and 0.01 s, which corresponds to approximately 2.75 in (69.9 mm) of
displacement. The second slope range occurs between 0.01 s and 0.09 s and corresponds
to failure of the lateral member/shelf, as well as pull down of the AT plate. Finally,
between 0.07 s and 0.09 s, the last slope corresponds to pull out of the corner post from
the AT plate. This shows the lag time in response from the position of TSP3, TSP4, and
TSP5. The nearest string potentiometer to the AT plate, TSP5, shows disturbances from
the AT plate before the further removed string potentiometer, TSP3, shows disturbances.
The test data has only been plotted to just after failure of the AT plate attachment; data
past that time is unreliable due to failure of the gauges.

The maximum measured displacement of the corner post near the point of impact before
separation of the AT plate attachment, taken from Figure A-5, is approximately 19 in
(483 mm). Upon pull out, some elastic recovery and post-test measurement show that the
corner post was permanently deformed by 18.5 in (470 mm).

Figure A-6. Gauge Locations at the End Structure and Under Structure of a 1990s Design Carbody

Measured strain provides information about the load transfer and timing of events. Figures A-6 through A-17 show the locations of strain gauges and the measurements recorded at these locations. Figure A-6 is a series of photographs of the 1990s design end structure and understructure, with squares representing the approximate strain gauge locations.

Figures A-7 and A-8 show the combined results from the strain gauges placed at the base as well as at the top of the corner post. The accompanying photograph shows the approximate locations of these gauges on the corner post. After initial contact of the coil with the corner post, the load built up, reaching a peak around 0.02 s. After that time, the central hinge fully forms, and the secondary hinge at the base of the post grows. The

corner post completely pulls out of the AT plate at 0.07 s. After that time frame the post is allowed to fully rotate at the corner post—buffer/end beam connection until the coil forces the corner post into the back partition wall. The strain gauge information at the base of the corner post experienced an initial offset, but the shape of the strain time curve is consistent with that obtained from the top of the corner post.
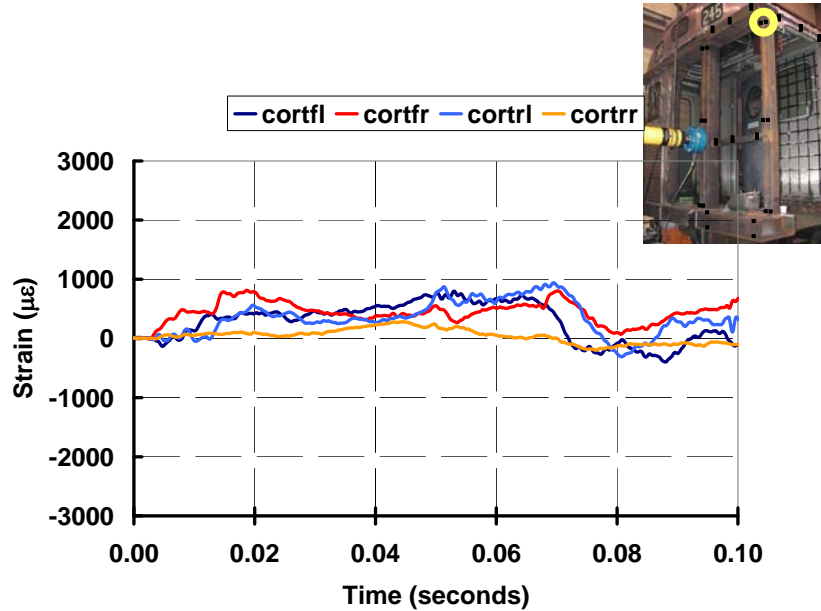

Figure A-7. 1990s Design Corner Post Strain Gauge Measurements—Top
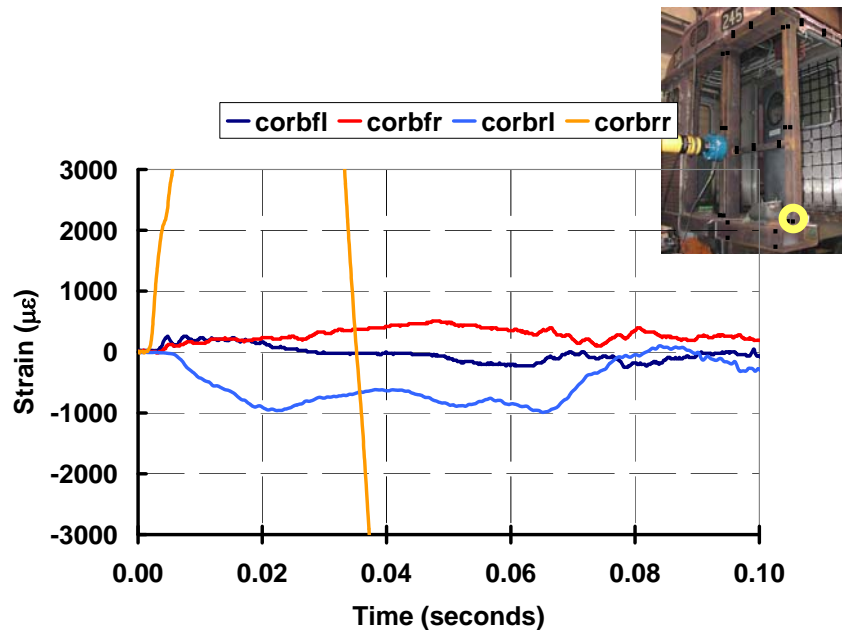
Figure A-8. 1990s Design Corner Post Strain Gauge Measurements—Bottom

Figures A-9 through A-11 show the information obtained using the strain gauges placed on the AT plate. Impact is registered with a slight delay in timing. The first set of peak strains occur between 0.01 s and 0.02 s. It is during this time frame that only the post deforms. At 0.04 s the AT plate starts to form a hinge at the connection with the collision post. The photometric analysis also shows that this time also corresponds with the frangible box structure upon which the steel coil rested strikes the buffer/end beam. The plastic hinge continues to evolve until the corner post pulls out of the AT plate between 0.07 and 0.08 s. The smallest strains measured occurred in the middle of the AT plate.
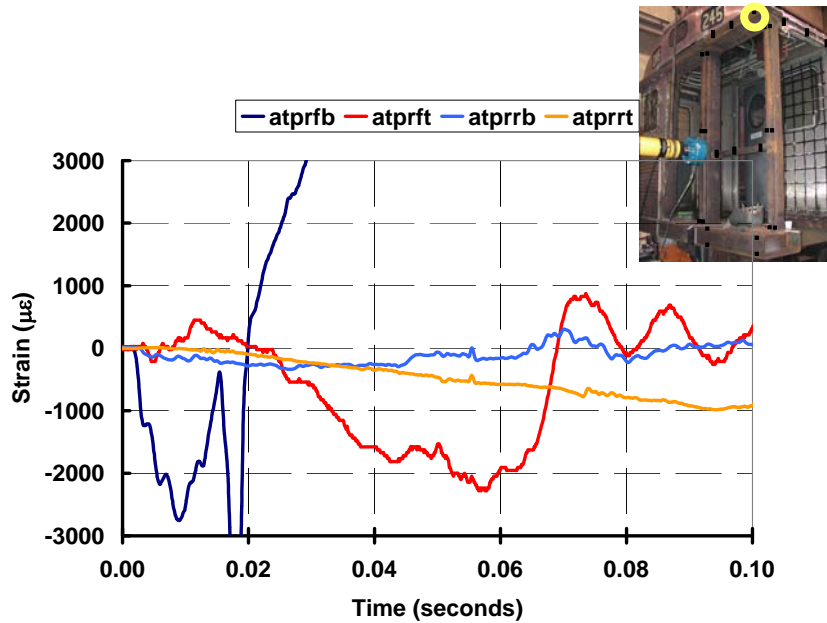
Figure A-9. 1990s Design AT Plate Strain Gauge Measurements—Right
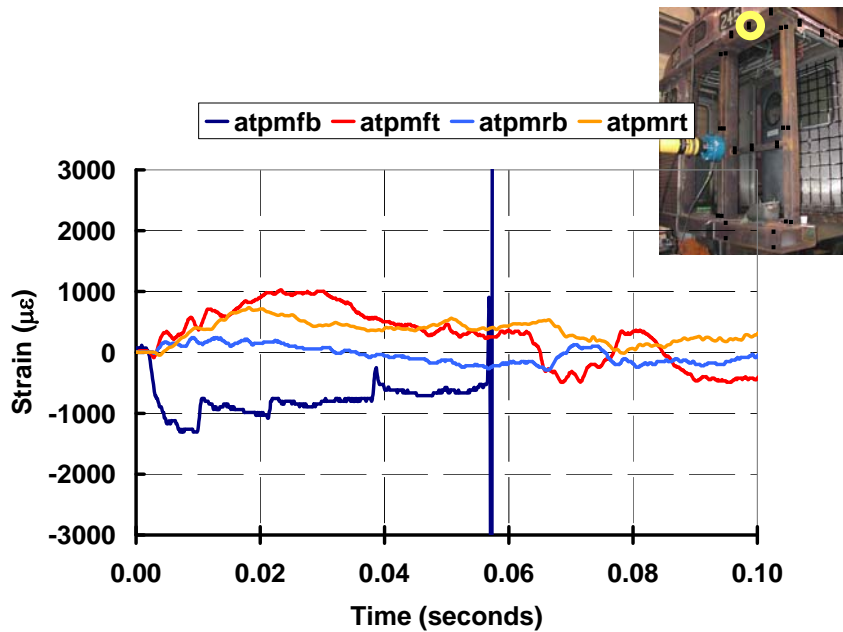
Figure A-10. 1990s Design AT Plate Strain Gauge Measurements—Center
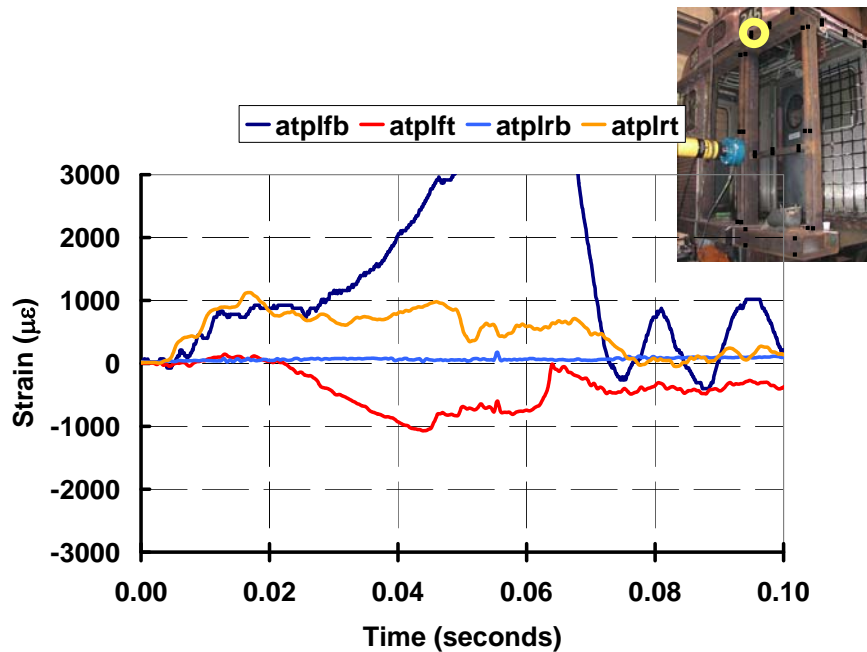
Figure A-11. 1990s Design AT Plate Strain Gauge Measurements—Left

Figures A-12 through A-14 show the strains measured at the top, middle, and base of the collision post. Strains build up upon initial contact with the load first being transferred from the lateral member/shelf to the middle of the collision post, then proceeding through the AT plate, and finally through the end beam. The end beam is very stiff and acts like a

fixed boundary condition on the corner post, while the AT plate acts more like a longitudinally pinned connection with a rotational spring. Between 0.02 and 0.05 s, the lateral member shelf experiences a combined tensile and shear load as it tears out of its connection to the collision post. The lateral member/shelf completely fails at 0.05 s. Load is then only transferred through the AT plate and the buffer/end beam into the collision post. The strains are greatest at the base of the collision post due to the long moment arm through which the longitudinal load is transferred from the top of the collision post through the AT plate. Pull out of the corner post is very apparent in all measurements due to the rapid change in slope of the strain between 0.07 and 0.08 s.
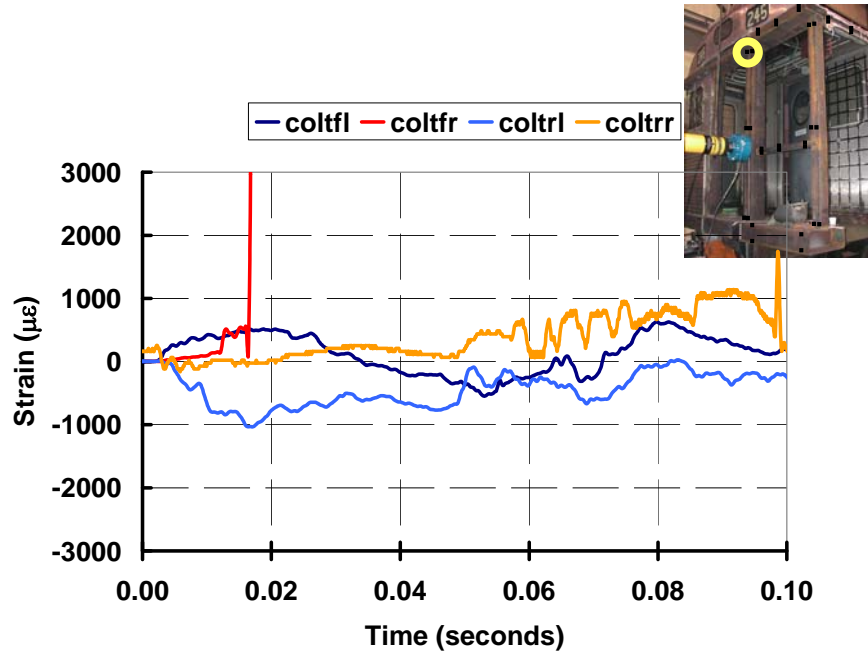
Figure A-12. 1990s Design Collision Post Strain Gauge Measurements—Top
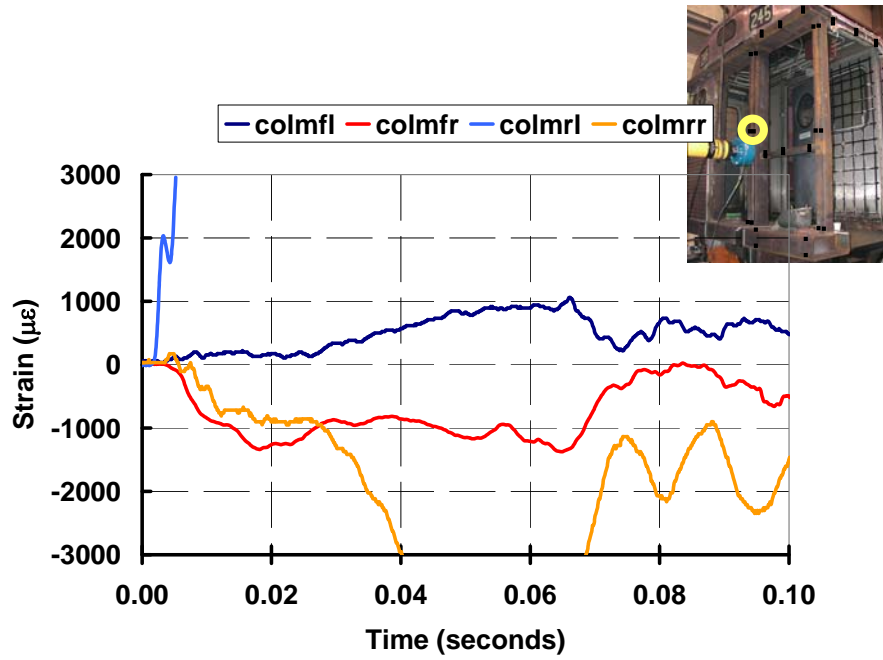
Figure A-13. 1990s Design Collision Post Strain Gauge Measurements—Middle
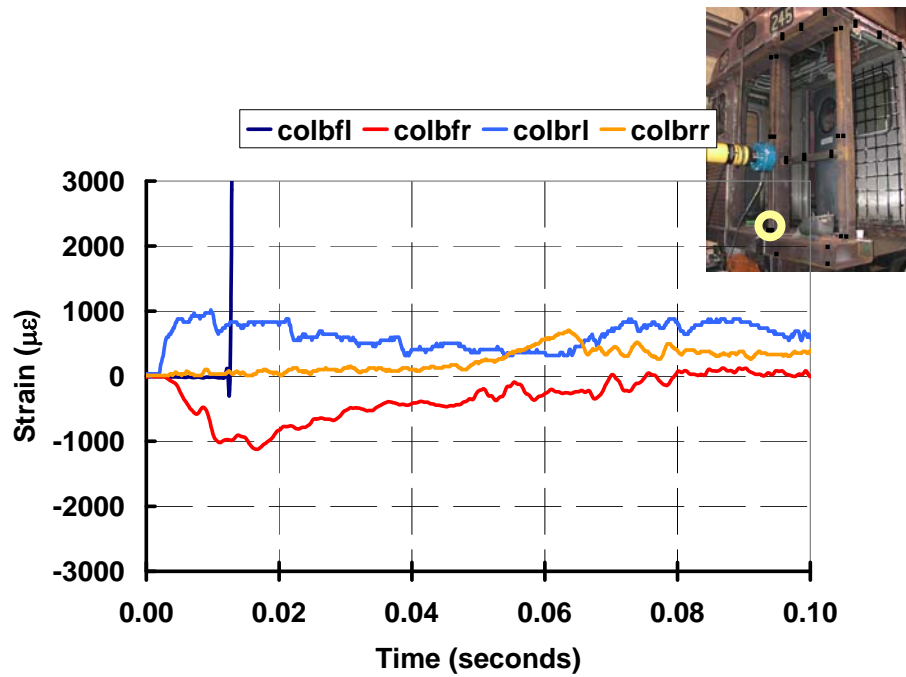
Figure A-14. 1990s Design Collision Post Strain Gauge Measurements—Bottom

Figures A-15 through A-17 show the strain gauge measurements taken on the draft sill for the 1990s design. The magnitudes of strains are largest near the point of loading and progressively decrease further back into the car structure. The load goes into the draft sill as a bending load with compressive strains measured on the side closest to the loading point and tensile strains on the opposite side of the draft sill. The load builds up gradually to a peak in the first 0.02 s. Pull out of the corner post is again apparent because of the rapid change in strain in the same time period as discussed previously.
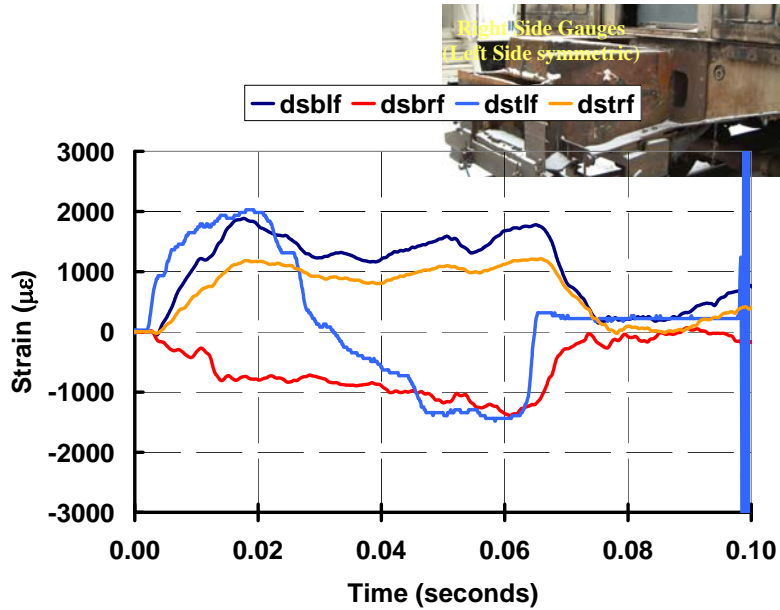
Figure A-15. 1990s Design Draft Sill Strain Gauge Measurements—Front
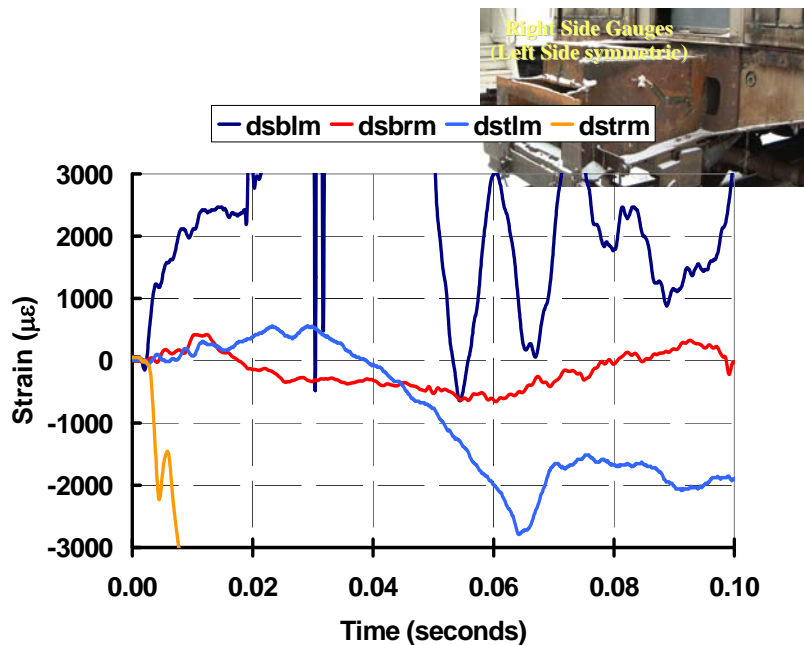
Figure A-16. 1990s Design Draft Sill Strain Gauge Measurements—Middle
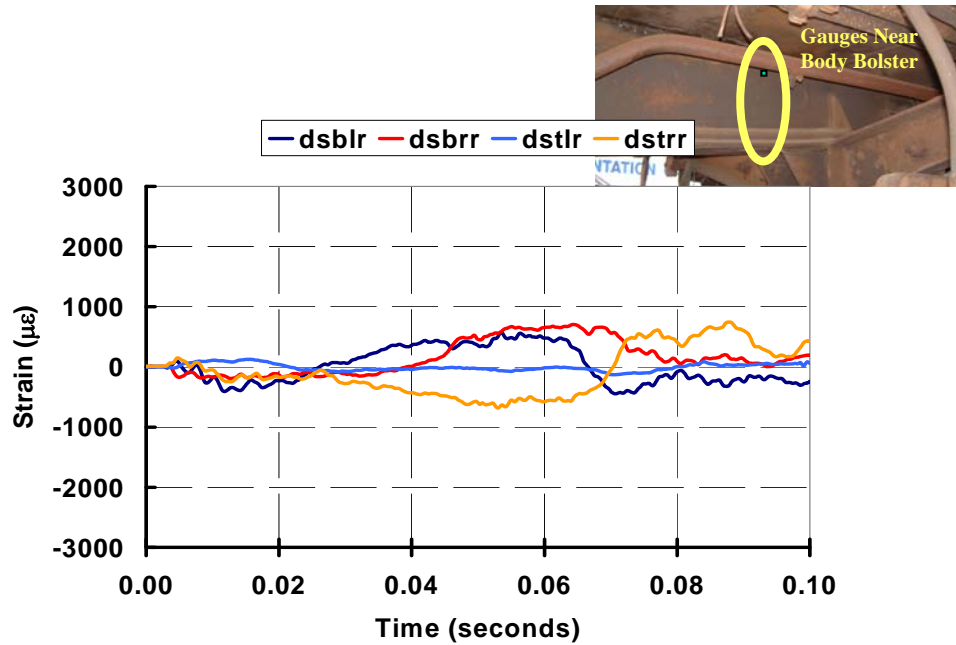
Figure A-17. 1990s Design Draft Sill Strain Gauge Measurements—Rear

Figure A-18 shows three still photographs taken from a high-speed movie film of the 1990s design grade crossing test. The first frame shows the coil and corner post at the instant of impact. The second frame shows the coil and cab car just before complete failure by pull out of the corner post from the AT plate at approximately 0.08 s. At this time the post has displaced inwards 18 in (457 mm). The third frame shows the coil and cab car after 0.09 s and 19 in (483 mm) of displacement of the corner post. Just below those three frames are results from the pre-test analysis with material failure for the mode shape of the cab car end structure at the same times and nearly the same displacements.
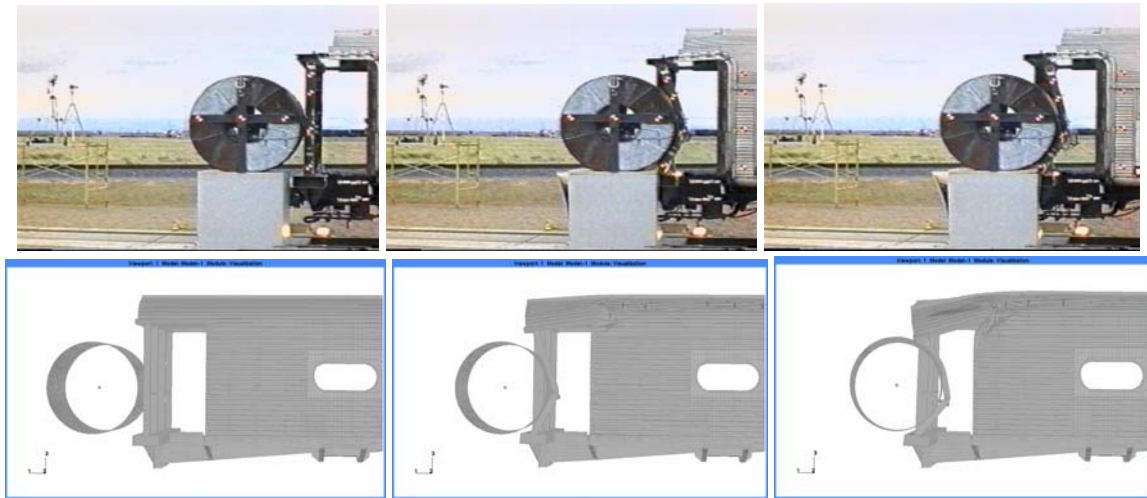
Figure A-18. Measured and Pre-Test Predicted Mode of Deformation, 1990s Design, Up to Corner Post Upper Attachment Failure

The predicted deformation mode shape matches that observed in the test but for one detail. In the third frame, the frame from the test shows only a small amount of vertical distortion of the roof above the upper rear corner of the near-side doorway, while the frame from the model predictions shows more distortion of the top of this doorframe. This difference in mode may result from the changes in the attachment of the end frame to the original car structure, as well as the strain-to-failure criterion used. In addition, the difference in length of roof material is not present on the test vehicle. The original model integrally attached roof sheeting to the AT plate, which experiences a counterclockwise torque as the AT plate is pulled downwards. To maintain compatible deformations, this load is reacted above the doorframe where a plastic hinge is formed in the cant rail, the roof sheeting, and the hat sections on top of the roof.

Despite the minor differences discussed between the pre-test, post-test, and test measurements, very good agreement exists overall in terms of total energy consumed through plastic deformations, as well as modes of deformation and failure. This information is then provided as input into the CD models discussed in the next section. Further work is currently underway to develop a better engineering failure algorithm that can be incorporated into the FE solver. The goal of this work is to be able to account for failure in a component by combining not only strain states but the stress states as well [11][12].

Figure A-19 shows a still photograph taken from the high-speed film. This frame shows the failed upper attachment of the corner post. The photograph on the right is a plot of the deformed mesh from the revised FE analysis. The coil has been removed for clarity. The results of the revised analysis are in close agreement with the test observations. The pull out mode of failure has been captured using the model with a refined mesh. A shift has occurred in the time it takes for the pull out failure to occur as noted in the string potentiometer discussion.
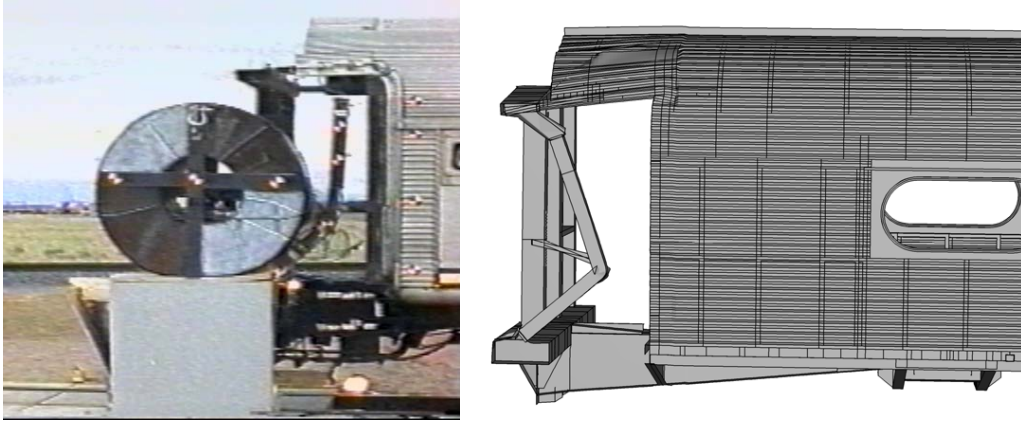
Figure A-19. Measured and Post-Test Predicted Mode of Deformation, 1990s Design, Corner Post Upper Attachment Failure

SOA Design

Figure A-20 shows the pre-test predictions for the force-crush characteristic for the SOA design. The model was exercised with and without material failure. The model predictions with material failure nearly overlay the test results. Similar to the results discussed with the 1990s design, a small phase shift occurred in the timing of events. The peak load caused by the initial contact occurs almost instantaneously for the FE model and is higher than what occurs in the test measurements. As seen from the test measurements, a finite rise time occurs for the initial load, and the peak load is smaller. In the test measurements and the crush model results, the initial peak is associated with the formation of the central plastic hinge on the corner post. The second and third peaks with their associated load plateaus correspond to the formation of the plastic hinges at the corner post/end beam connection and the corner post/AT plate connection respectively. The difference between the crush models with and without failure is apparent after 4 in (102 mm) of crush. The model without failure considerably overpredicts the load after 6 in (152 mm) of crush, but has a similar unloading slope as observed in the test. The model with failure predicts slightly higher loads after 7 in (178 mm) of crush, but the same maximum crush distance as observed in the test. The rate of unloading predicted with the no failure model, however, is slower than observed in the test.
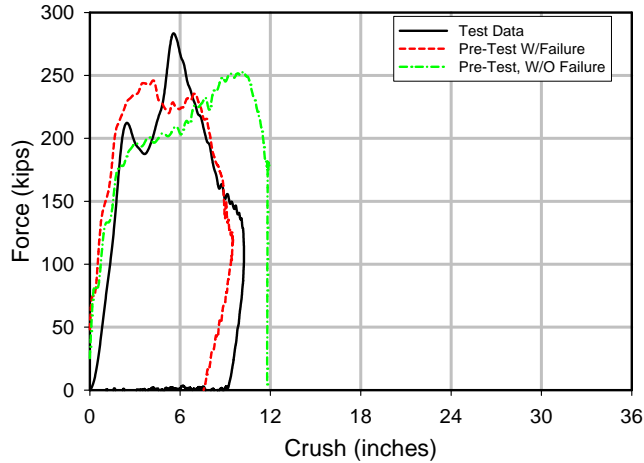
Figure A-20. Measured and Predicted Force-Crush Characteristic, SOA Design

Figure A-21 shows the force-time comparison of the test measurements and the crush model with failure. The force-time trace from the test was derived using the resultant deceleration taken from the nine-accelerometer array on the coil multiplied by the coil mass. These results are unfiltered. Despite the minor inconsistencies between the test measurements and the crush model results, very good agreement exists. The phase shift experienced in the model is not surprising given the simplicity of the failure criterion used. In the FE model, when elements fail they are removed from the calculation. When too much material is removed, the predicted response in the FE model is softer than the response seen in the test.
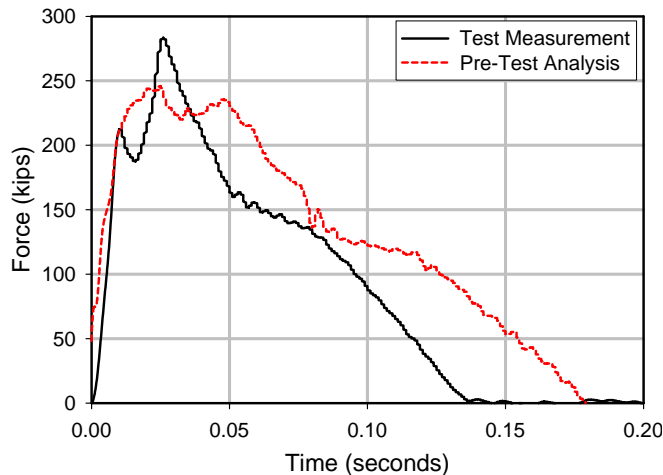
Figure A-21. Measured and Predicted Force-Time Histories, SOA Design

Figure A-22 shows a comparison of the measured string potentiometer longitudinal displacement (solid line) with that predicted before the test (dashed line). The crush model results reflect the average displacement taken at the centroid of the center element at the appropriate height on the corner post. The results presented are for the same string potentiometers as discussed in the 1990s design discussion above. Initially, the displacements predicted in the crush model are less than those measured in the test at a given point in time, which means the response predicted is stiffer. However, when failure is predicted to start in the model, the structural stiffness decreases as a result of

38

too much material being removed during element removal. While the peak predicted displacements are larger in the model than predicted by the tests, the unloaded final displacements are close. The flat lines at the end of each test result plotted show the final position of the post after rebound of the coil has occurred. The test measurement taken at the point closest to the point of initial contact is 8 in (203 mm) while that predicted by the model is 8.5 in (215 mm).
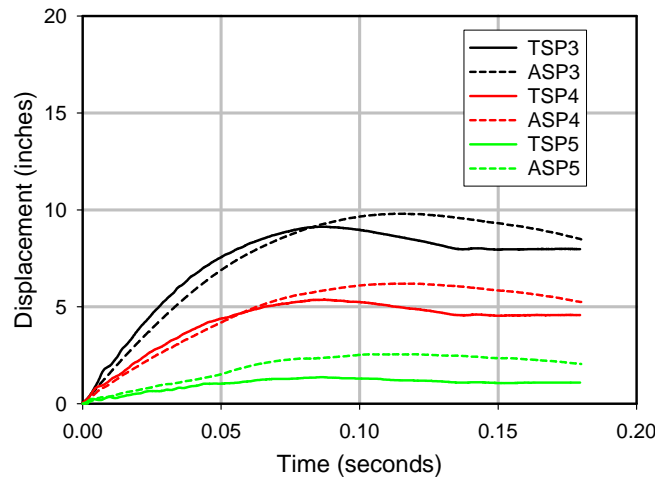
Figure A-22. Measured and Predicted Longitudinal Displacement-Time Histories on SOA Corner Post

Figure A-23 shows three still photographs taken from a high-speed movie film of the test of the SOA design. The first frame shows the coil and corner post at the instant of impact; the second frame shows the coil and the cab car after approximately 0.03 s and 5.25 in (133 mm) rearward displacement of the corner post. The third frame shows the coil and the cab car after approximately 0.08 s and 9 in (229 mm) of displacement of the corner post. Just below those three frames are results from the pre-test analysis with material failure for the mode shape of the cab car end structure at the same times and nearly the same displacements. The predicted mode shape closely matches the mode shape observed in the test. Slightly more vertical distortion of the roof occurs above the upper trailing corner near-side doorway predicted by the model than seen in the test result. Similar late changes in the attachment of the end frame to the original car structure were made in the SOA design as in the 1990s design; however, the SOA design is not as sensitive to these changes, since the corner post was attached to the top and bottom plates of the AT plate. The additional strength of the attachment in the SOA design forced the AT plate to deform downward, rather than allowing the attachment to fail, as it did in the 1990s design.
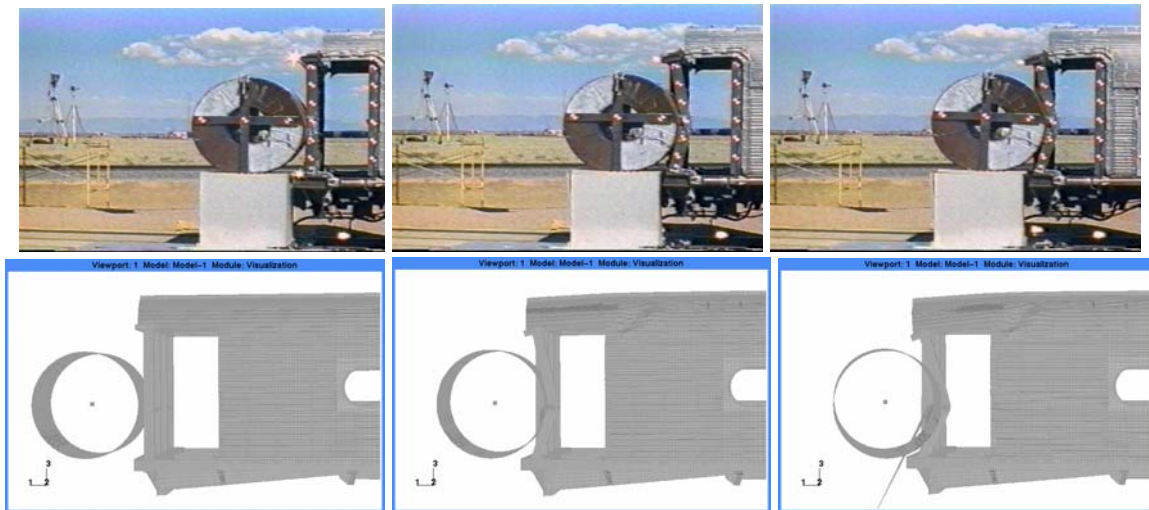
Figure A-23. Measured and Pre-Test Predicted Mode of Deformation, SOA Design

Despite the minor differences discussed between the pre-test and test measurements, overall very good agreement exists in terms of total energy consumed through plastic deformations, as well as modes of deformation and failure. This information is then provided as input into the CD models discussed in a later section. The next section discusses in greater detail the areas that experienced material failure for both sets of tests.

Material Failure

As shown in the force-crush characteristics in Figures A-3 and A-20, modeling of material failure was necessary for accurate prediction of the force-crush characteristic. Material failure occurred at multiple locations in both tests and under a range of stress states. Material failure was sufficiently extensive in the test of the 1990s design to allow separation of the top of the corner post from its attachment to the AT plate and separation of the lateral member/shelf from the corner post.

In both tests the corner post acted largely as a fixed-pinned beam that is overloaded. A plastic hinge formed early in the test near the center of impact. As the test progressed, the corner post bent into a V, which put a significant tension load on the corner post. Both the upper and lower attachment of the corner post had to support the shear load from the coil and the tension load due to the bending of the beam. The end beam did not visibly plastically deform, and the floor attachment acted as a fixed connection. The AT plate and the cant rail did deform downward, and consequently the roof connection of the corner post acted as a pinned connection. Figure 9 in Section 5 shows a post-test photograph of the deformed shape of the corner post.

Material failure occurred in the 1990s end frame design test at the attachment of the corner post to the end beam, at the attachment of the corner post to the AT plate, and at the attachment of the lateral member/shelf to the corner post. Figure A-24 shows close-ups of the material failures at these locations. The left-hand photograph shows the failure that occurred at the base of the corner post/end beam connection. As the central hinge in the corner post rotated and pushed inwards, large bending and tensile stresses developed

on the top plate of the end beam on the impact side, while large bending and compressive stresses devolved on the aft side of the connection. The failure of the top plate is in the parent material of the sheet just outside the weld, effectively in the heat-affected zone. The photograph in the center shows the top of the corner post, which pulled out of the AT plate during the collision. The stress state to cause this failure mode was almost a pure state of shear. The right side photograph shows the attachment of the lateral member/shelf to the collision post. This connection failed due to the combination of bending and shear.

Figure A-24. Post-Test Photographs of Material Failure in 1990s Design, Corner Post Connection to End Beam, Failed Connection at Top of Corner Post, and Failed Connection to Shelf on Collision Post

Material failure occurred in the SOA end frame design test at the connection of the corner post to the end beam, at the attachment of the AT plate to the cant rail, and at the attachment of the lateral member/shelf to the corner post. Figure A-25 shows photographs of the material failure at these locations. As the central plastic hinge rotated and displaced inwards, large tensile and bending stresses developed on the impacting side of the corner post at its connection with the end beam, while large bending and compressive stresses developed on the aft side of the corner post. Unlike the failure mode experienced by the 1990s end frame design, this time the parent material in the corner post, rather than the end beam failed. The failure progressed nearly the full depth of the post. No upward bending in the end beam occurred in the upper flange because this design had the corner post penetrating through both the upper and lower flanges of the end beam, and the end beam was reinforced by the closed side sill that extended all the way forward from the aft operator's compartment wall. The necking/cup-cone deformations present on the pulled-out post and the in-situ post are indicative of a tensile failure that then proceeded to open further as a result of the combined tension and bending. The material failure that occurred at the AT connection with the cant rail was in the region of a weld. This failure mode was caused by the rotation of the AT plate as the central hinge displaced inwards, and a prying load ensued between the AT pad connection point and the cant rail. Finally, the last area with material failure is at the connection point of the bulkhead sheet with the lateral member/shelf and the collision post. As the coil penetrated inwards during the collision, the bulkhead sheet and the lateral member/shelf transmitted load to the collision post. Large tensile and shear stresses developed at this connection point. The failure proceeded from the outside inwards and downwards between the collision post and bulkhead sheet weld.

Figure A-25. Post-Test Photographs of Material Failure in SOA Design, Corner Post Connection to End Beam, AT Plate Connection to Roof Plate, and Shelf Connection to Collision Post

As described earlier, currently material failure is modeled in many FE analysis packages using a simple strain-to-failure criterion. When the total strain on an element reaches an input value, that element is removed from the mesh. This approach works well when the principal cause of material failure is tension and the extent of material failure is limited. Limitations of the current approach to modeling material failure include that materials fail at different strains in tension, compression, and shear [11], and that once material failure has initiated, lower strain is needed to propagate the failure [13].

Sophisticated application of current FE analysis packages allow these limitations to be overcome to some degree. By first running the model without material failure, the areas of high strain and potential material failure can be found. The model can then be run again with the parameters associated with material failure adjusted to account for the stress state of the high-strain areas. If the three-dimensional stress state of two or more high-strain areas substantially differs (for example, one in tension and one in compression), then the model can be substructured and different material-failure parameters applied to each substructure. An effort is currently underway to better understand material failure under a wide range of strain states and to develop algorithms that more accurately predict material failure [12].

A.3. Collision Dynamics Model

CD models were created using ADAMS software [11] to evaluate the collision results. This three-dimensional model predicts the crush of the cab car and the three-dimensional motions of the coil and the cab car.

The CD model is a lumped-mass representation of the cab car and the steel coil. As shown in Figure A-26, the model consists of a series of masses connected by nonlinear springs. The longitudinal springs use the force-crush characteristic obtained from an FE model, which simulates the crush behavior of the end structure. Set with the appropriate initial conditions, the CD model provides the gross motions of the cab car and the coil and the amount of deformation at the impacting end of the cab car. The lateral deflection of the coil is modeled in a similar manner as the CD model, developed for analyzing an

oblique collision of a locomotive with a container, which in turn evolved from the CD model developed for analyzing an oblique collision of a locomotive-led consist with a cab car-led consist [14].
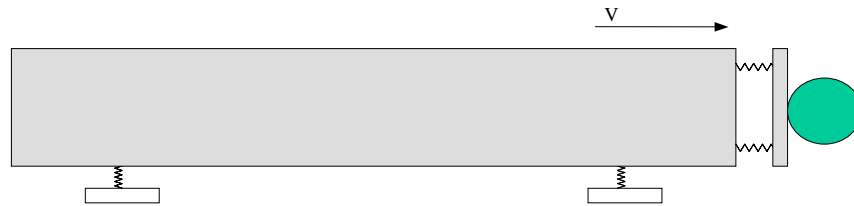

Figure A-26. Schematic of Lumped-Mass CD Model

Modeling Parameters

As shown in Figure A-26, the impacting end of the passenger car is joined to the main body by two springs, each representing half the symmetric structural behavior of the carbody end. These characteristics are defined by nonlinear characteristics that are derived from the FE model.

In the model, a spherical rigid body represents the steel coil. When the colliding bodies try to penetrate each other, the contact force is modeled by an impact element that uses a compression-only, nonlinear spring-damper function to calculate the resultant collision force. The impact stiffness and damping coefficients are 1.0E+06 lb/ft and 2.0E+04 lb-s/ft, respectively.

The truck elements account for the wheel to rail interaction. They allow for both vertical and lateral forces with the ground. Accordingly, spring-damper elements are used between the truck and carbody to represent the secondary suspension.

The mass properties for the carbody and coil in the model are defined as shown in Tables A-1 and A-2.

Table A-1. Vehicle Mass Properties

Property	*1990s Carbody*	*SOA Carbody*	*Truck*	*Corner Post*
Mass (lbm)	33,800	35,018	12,000	250
Centroidal Roll (lbm-ft^2)	9.68E+05	9.68E+05	3.55E+04	8.16E+02
Centroidal Pitch (lbm-ft^2)	2.22E+07	2.22E+07	1.08E+05	8.16E+02
Centroidal Yaw (lbm-ft^2)	2.25E+07	2.25E+07	9.28E+04	8.16E+02

Table A-2. Steel Coil Mass Properties

Property	*Coil*
Mass (lbm)	41,300
Axial Inertia (lbm-ft^2)	2.25E+05
Transverse Inertia (lbm-ft^2)	1.60E+05

Force-Crush Behavior

The combined results of the FE and CD models provide the predictions necessary to create a focused full-scale test. The FE model established the limits within which the collision must occur. The CD model used the force-crush curves from the FE model before the test to estimate the corresponding collision speeds bounded by the desired deformation. The curves were entered into the CD model as the non-linear force-crush characteristics of the specific end structures. The CD model was used to estimate the extent of crush of the cab car as a function of the impact velocity.

Following the full-scale test, the force-crush characteristics input into the CD model can be updated with the test measurements. The pre-test prediction for the 1990s cab car force-crush characteristic proved accurate up to about 12 in (305 mm). After this point in the full-scale test, the corner post pulled out of its upper attachment at the AT plate. After the test, the input for the 1990s CD model was updated with force-crush from the processed test data. With this one change, the 1990s model results compare closely with the test results for the amount of cab car crush and for the gross motions of the cab car and coil. The SOA cab car test went nearly exactly as simulated, with approximately 9 in (229 mm) of longitudinal deformation occurring in the corner post. Consequently, the input to the SOA CD model did not require post-test changes. Figures A-27 and A-28 show the pre-test and post-test force-crush curves.
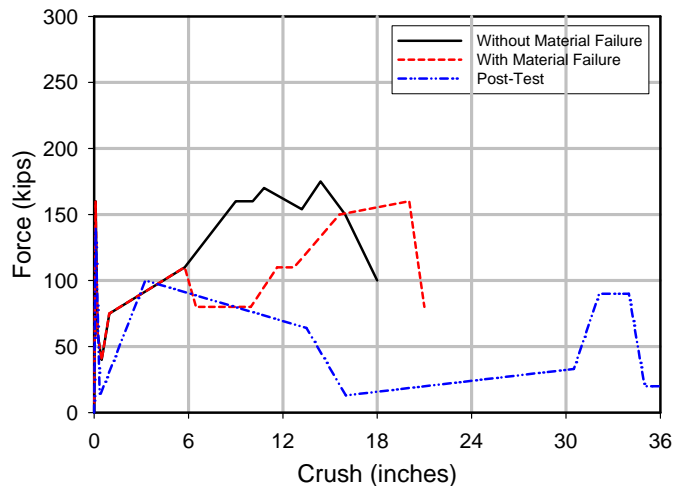

Figure A-27. 1990s Force-Crush Characteristics
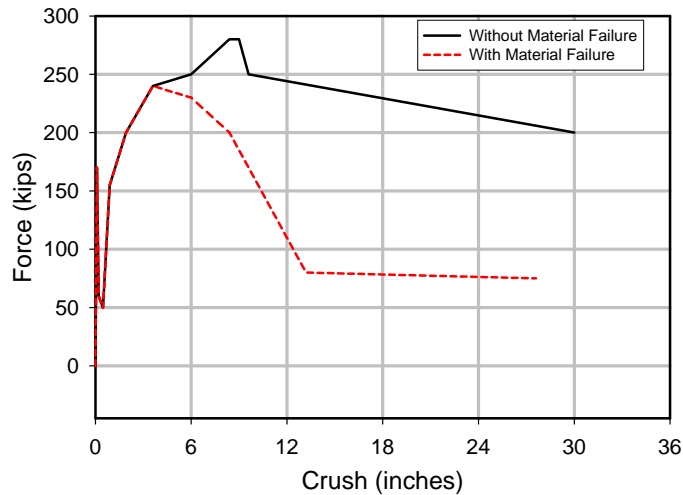
Figure A-28. SOA Force-Crush Characteristics

Gross Motions

During both tests, the cab cars impacted the heavy object, demolished the frangible table, and continued along the track at a decreasing velocity. In the 1990s cab car impact test, the impact of the heavy object broke through the corner post. The steel coil became momentarily embedded in the end structure and then fell beside the cab car. During the SOA cab car collision, the impact of the steel coil caused about 9 in (229 mm) of longitudinal deformation in the corner post, after which the coil fell from the cab car onto the track. During the impacts, when the coil and the car were in contact, the lateral and vertical displacements of the coil and the car were small—less than 1 in (25.4 mm). The yaw displacements of the coil, as it deflected from the cab car, were significant in both tests—approximately 19 degrees for the 1990s cab car test and 4 degrees for the SOA cab car test. With the revised input force-crush characteristic, the predictions of the CD model with the 1990s design end structure are in close agreement with the test measurements, including the yaw of the coil. The predictions of the CD model of the test of the cab car with the SOA end frame are also in close agreement with the test measurements.

The deceleration records for the two impact tests are displayed in Figures A-29 and A-30, plotted with corresponding data from the CD model. While in contact, the coil and the carbody acceleration histories are essentially mirrors of each other, scaled according to weight.

45
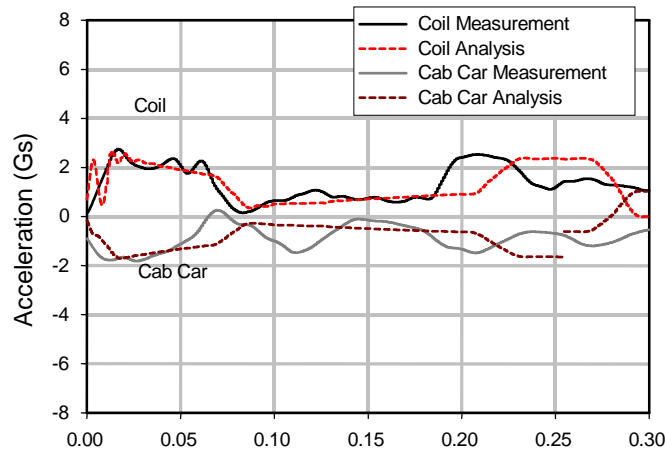
Figure A-29. Longitudinal Decelerations of 1990s Cab Car
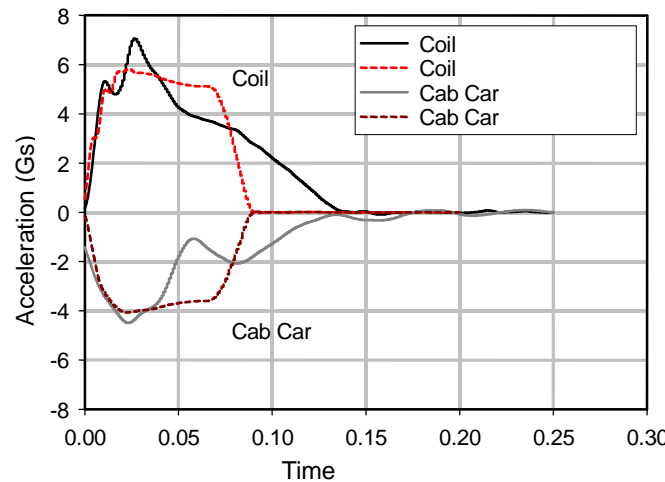
Figure A-30. Longitudinal Decelerations of SOA Cab Car

The cab car that had been modified with the 1990s end structure had previously been used in the single car full-scale test [15], and the cab car that had been modified with the SOA end frame had been the lead car in the two-car full-scale impact test [16]. Since the back ends of both cars were open during the grade crossing tests, the body shells were relatively free to vibrate. As a result, the cab car data had to be filtered with a lower bandwidth filter. The cab car data was filtered with a CFC 15 filter, while the coil data was filtered with a CFC 60 filter [17]. The CFC 15 filtering resulted in less than 1 percent error in the displacement of the cab car as integrated from the accelerometer data, for both tests [18].

The CD model reproduces the test longitudinal carbody accelerations very closely. It captures the initial peak deceleration due to impact followed by a reasonable estimate of the carbody motions. From Figures A-21 and A-22 above, it is apparent that the data extracted from the coil instrumentation has significantly less noise than the carbody

46

instrumentation. Consequently, the coil acts effectively as a force transducer for comparison and revision of test data with the model results.

The difference between the 1990s and SOA designs is evident in these results. The SOA design displays higher accelerations due to the increased strength of the end structure required by the revised 1999 APTA standards. The 1990s design receives lower accelerations over a longer time period, indicative of the prolonged deformation. The failure is seen in the drop off of acceleration at around 0.1 s, as the corner post gives way and briefly looses contact with the coil.

The raw accelerometer data was integrated to produce the velocity-time histories. Figures A-31 and A-32 show the comparison of the model results to the test data. The CD models accurately predict the gradient of speed and final time at which the colliding bodies come to a constant velocity.
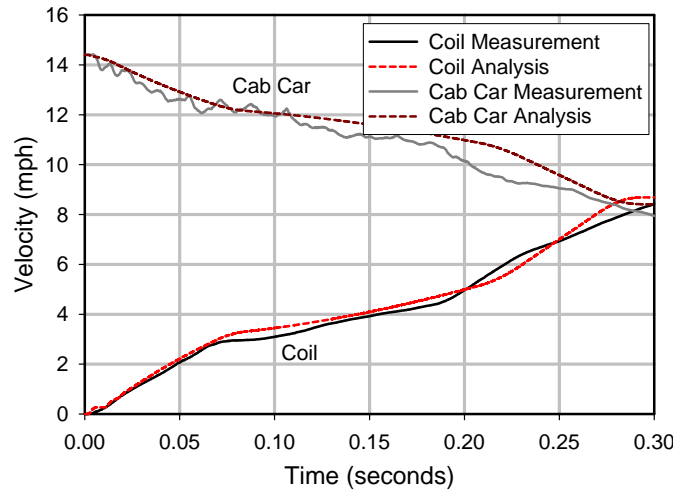

**Figure A-31. Velocity-Time History of 1990s Cab Car**
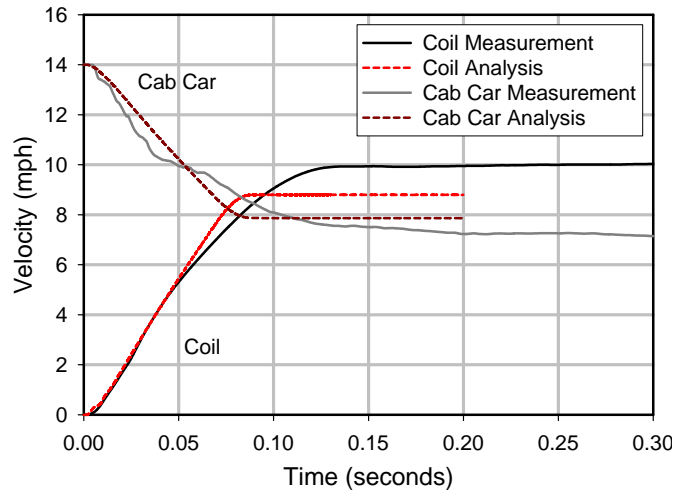
Figure A-32. Velocity-Time History of SOA Cab Car

In both collisions the trains arrive at a post-impact velocity of about 8 mph (12.8 km/h). The SOA cab car impact takes approximately half the time of the 1990s cab car impact to reach this constant velocity due to the increased stiffness of the SOA design.

Accelerometers measuring lateral and vertical carbody motions were analyzed, and these motions were found to be negligible. The lateral and vertical displacements of the cab car and coil were all less than 1 in (25 mm) while they were in contact, for both tests. Peak lateral carbody accelerations ranged from 2-3 Gs in the first 0.03 s and are primarily attributed to the initial impact of the heavy object at the corner, causing a slight moment about the train's center of mass. While these lateral forces were identified to be of a characteristic pattern seen in larger scale collisions in which derailment occurred, the magnitude of the lateral forces was well below a state of concern [19]. After initial impact, lateral accelerations were less than 1 G.

The CD model also accurately predicts the yaw of the coil. Figures A-33 and A-34 show comparisons of the coil's rotational acceleration about the vertical axis. The coil yaw acceleration is reflective of the pattern of the contact force. In the 1990s cab car test, the coil shows a peak rotational acceleration of about 22 radians per second squared. The CD model predicts a yaw acceleration of about 20 radians per second squared. The second significant peak, occurring at about 0.2 s, shows when the coil breaks through the corner post and impacts the passenger compartment wall. This second peak in the yaw acceleration occurs because the contact point on the coil is different for the rear of the doorframe than it is for the corner post. The CD model currently does not account for this shift, although it could be modified. The SOA cab car comparison shows that the CD model follows the slope of the test data very precisely. Double integrating the test data produces a final rotational displacement of about 20 degrees. The still shots shown in Figure A-35 depict general visual agreement with the position of the rotated coil.

48
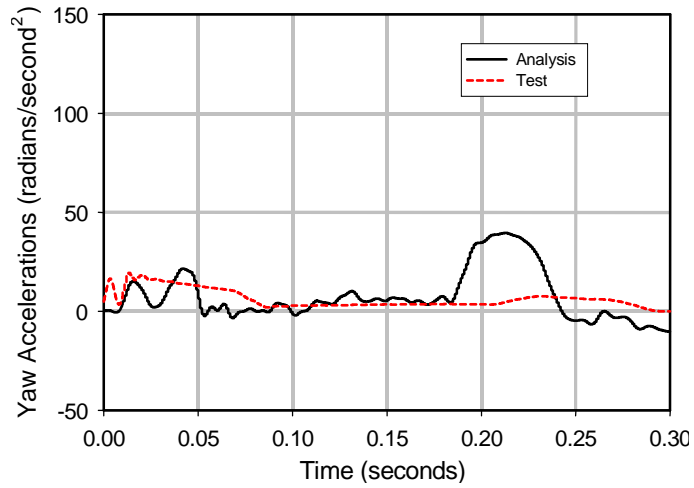
Figure A-33. Comparison of Coil Yaw Acceleration, 1990s Cab Car Impact, Test Data, and Analysis Results
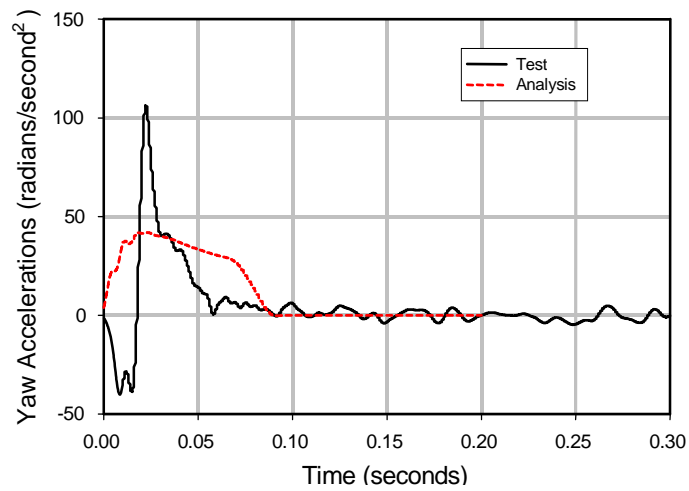
Figure A-34. Comparison of Coil Yaw Acceleration, SOA Cab Car Impact, Test Data, and Analysis Results
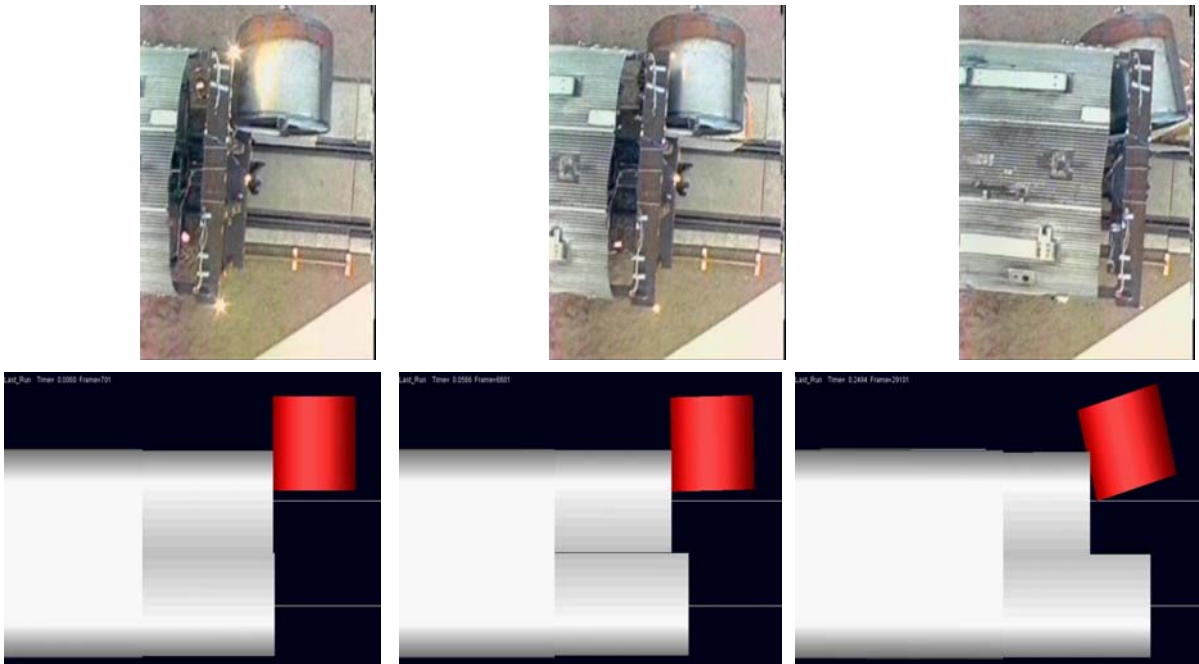
Figure A-35. Still Photographs of CD Simulation and 1990s Full-Scale Test

The CD models estimated the gross motions of the objects with relative accuracy. Figure A-35 shows still shots from an overhead view of the CD simulation in comparison with the high-speed camera of the 1990s full-scale collision. The pictures show the position at which the coil:

- Initially impacts the train (indicated by the flash of lights on the side of the passenger car)
- Breaks through the corner post
- Impacts the cab wall

A.4. Processing of Test Data

All post-processing of test data follows the recommendations of SAE J211-1, Instrumentation for Impact Tests [17]. The objective of post-processing the data is to correct time relative to initial collision impact, scale, and filter data, and to perform mathematical operations required to produce the results needed to compare test measurements to model predictions.

The raw data collected from the accelerometers is processed in multiple ways to provide the most useful comparisons. The sum of the mass times the acceleration-time histories of the colliding bodies yields the active collision force. This gives a reasonable estimate of the contact force predicted by the CD models.

The accelerometer data is also used directly to analyze the gross motions of the colliding bodies. The acceleration-time histories are integrated to acquire the velocity and

displacement records. The impacting force-time history can then be plotted against the displacement, showing the force required to crush the end structure.

The raw accelerometer data recorded a noisy signal of the carbody's motion. To make reasonable comparisons of acceleration-time histories, the data is filtered to extricate some of the high frequency content caused by the suspension, structural connections, and accelerometer attachments. The filtered data shows the motion of the train as a rigid body. This data is compared to the motions produced by the CD models. Figure A-36 shows the filtering process implemented.

```
                        ┌─────────────────┐
                        │  Acceleration   │
                        │      Data       │
                        └─────────────────┘
              ┌───────────────┴──────────────────┐
              ▼                                   ▼
    ┌──────────────────┐              ┌──────────────────┐
    │   Butterworth    │              │   Butterworth    │
    │ 4-Pole Phaseless │              │ 4-Pole Phaseless │
    │  Digital Filter  │              │  Digital Filter  │
    │     at 180 Hz    │              │     at 180 Hz    │
    │ (from SAE J211-1)│              │ (from SAE J211-1)│
    └──────────────────┘              └──────────────────┘
              │                                   ▼
              │                        ┌──────────────────────┐
              │                        │    Integration of    │
              │                        │     Acceleration     │
              │                        │   to Velocity Using  │
              │                        │ Trapezoidal Integration│
              │                        └──────────────────────┘
              │                                   ▼
              ▼                        ┌──────────────────────┐
    ┌──────────────────┐              │    Integration of    │
    │   Acceleration   │              │     Velocity to      │
    │    Time-Trace    │              │   Displacement Using │
    └──────────────────┘              │ Trapezoidal Integration│
        ┊         │                   └──────────────────────┘
        ┊         └──────┐        ┌──────────┘         │
        ▼                ▼        ▼                     ▼
  ┌──────────┐    ┌──────────┐  ┌──────────┐   ┌──────────────┐
  │  Force   │    │ Occupant │  │ Velocity │   │ Displacement │
  │Time-Trace│    │Environment│ │Time-Trace│   │  Time-Trace  │
  └──────────┘    └──────────┘  └──────────┘   └──────────────┘
```

Figure A-36. Post-Processing Flowchart

The filtering process was guided by the recommendations of SAE J211-1, as well as the post-processing practices exercised in previous full-scale rail vehicle experiments. SAE J211-1 recommends frequency response classes for recording various components of full-scale data. A CFC 60 Butterworth 4-pole phaseless digital filter was used on the coil accelerometer data, and a CFC 15 filter was used on the carbody accelerometer data.

A representative accelerometer was determined to be located at the front side of impact on the draft sill. This location provided the most useful data because it was at the front of the train near the impact but behind the end structure and area of crush. Accelerometers located towards the rear of the train not only have a time delay in their signal but provided noisier data because of the greater influence of the rear end of the carbody, which did not have an end structure.

51

Post-processing of strain gauges and string potentiometers includes filtering and plotting for comparisons and checks of valid results. Post-test analysis of the high-speed film is valuable to document vehicle displacements for comparison with integrated accelerometer data and with model results.

Appendix B.
Test Requirements

B.1. Test Requirements

The following is taken from the draft specifications for a Cab Car End Structure, Volpe: Development of Conventional Passenger Cab Car End Structure Designs for Full-Scale Testing, 74431-S-001a, 20 June 2001.

- General. The vehicle ends designed and built to this specification will be used for full-scale testing. Therefore, it is important that the design facilitate measurements and observations to be made during the tests. The types of tests envisioned include: a) a single vehicle colliding with an object representing a grade crossing obstacle; b) a multiple vehicle consist colliding with the rigid surface; and c) a multiple vehicle consist colliding with a grade crossing obstacle. The tests will be conducted at TTC in Pueblo, Colorado.

- Visibility. The vehicle end shall be designed in such a way that it will be possible to view the collision and corner posts during crush deformation in the test. For example, parts of the roof and sides must remain open to facilitate viewing by cameras mounted on the ground or on the vehicle.

B.2. Test Instrumentation

The primary objectives of the grade crossing impact test instrumentation are to record the gross motions of the colliding bodies with sufficient accuracy to analyze and compare the data with model predictions. This is accomplished by instrumenting the cab car and coil with accelerometers, string potentiometers, and strain gauges, to record, respectively, structural accelerations, corner post and suspension displacements, and material strains to define the load path.

SAE J211-1 provides general guidelines for all data acquisition [17]. For the 1990s test, 120 data channels were required for the instrumentation. There were 52 accelerometers, 9 string potentiometers, and 80 strain gauges. For the SOA design, 132 channels were required for the instrumentation. There were 52 total accelerometers, 9 string potentiometers, and 92 strain gauges. Data was recorded at a sampling rate of approximately 8000 Hz. There was 1 second of pre-trigger data collection and 7 s of post-trigger data collection. A closure switch, located on the front of the impacting car, marked all the data with a reference point indicating the point of impact in each record.

Accelerometers are used to measure the carbody gross motions in three dimensions, as well as the pitch, yaw, and roll. Figure B-1 shows accelerometer locations. Accelerometers placed throughout the carbody also capture the bending and twisting about the carbody axis. All longitudinal accelerometers had a range of 200-1000 Gs, vertical accelerometers had a range of 100-400 Gs, and most lateral accelerometers were 200 Gs.
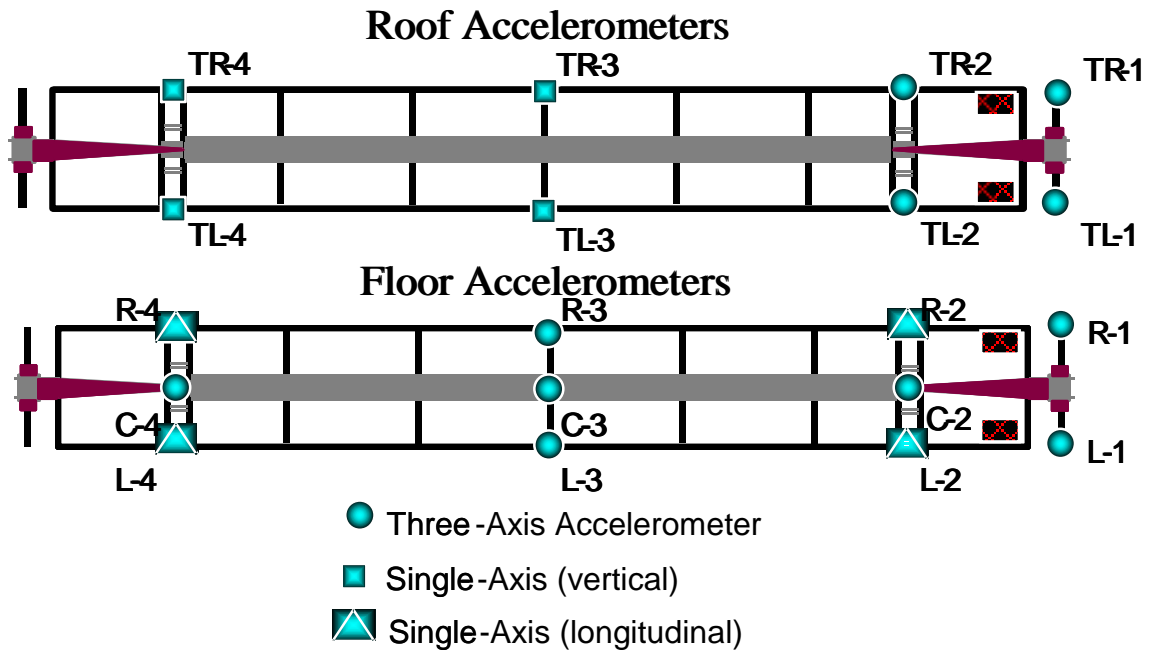

Figure B-1. Accelerometer Locations on Cab Car

Nine accelerometers were placed on the steel coil as shown in Figure B-2. All accelerometers had a range of 400 Gs. The following nine-array accelerometer configuration is used to provide a collection of data based on the local coordinate system of the coil [20]. This allows for the translational and rotational motions to be precisely measured.
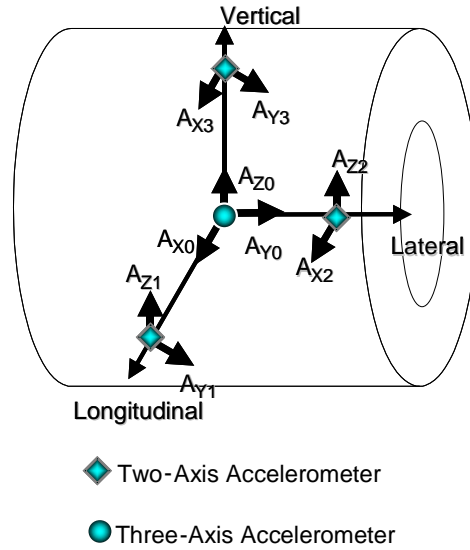
Figure B-2. Accelerometer Locations on Heavy Object

Nine string potentiometers were used in each test. Four string potentiometers were located on the passenger car between the body bolster and truck bolster to measure the relative vertical displacement of the suspension. Five string potentiometers were located on the corner post to measure its longitudinal deflection. Figures B-3 and B-4 show the locations and lengths of these displacement transducers relative to the corner post and the cab wall.
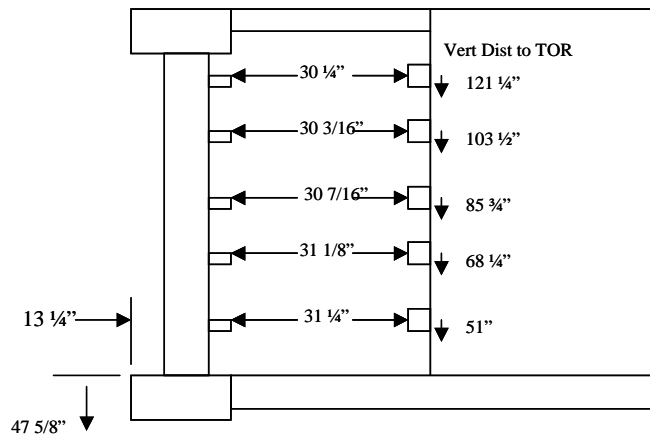

**Figure B-3. String Potentiometer Locations of 1990s Design**
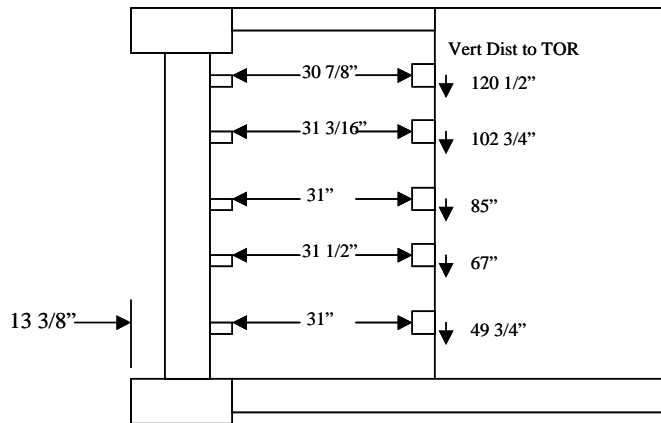
Figure B-4. String Potentiometer Locations of SOA Design

Strain gauges were used to determine the load path into the structure and to ascertain the timing of events for failure of components. The 1990s end frame design was instrumented with 80 uniaxial strain gauges, while the SOA end frame was instrumented with 92 uniaxial strain gauges. The structural elements of interest and the number of strain gauges placed on each component follow:

- The cant rail at the impact end of the cab car (12 uniaxial strain gauges).
- The draft/center sill at the impact end of the cab car (12 uniaxial strain gauges).
- The corner post (12 uniaxial strain gauges).
- The collision post (12 uniaxial strain gauges).
- The buffer/end beam (8 uniaxial strain gauges).
- The AT plate (12 uniaxial strain gauges).
- The lateral member/shelf below the window frame (12 uniaxial strain gauges).
- For the SOA design, 12 extra strain gauges will be required on the side sill that extends from the body bolster and connects with the buffer beam.

Figure B-5 shows schematically the locations of the strain gauges placed on the SOA design, which was retrofitted onto a Budd Pioneer cab car. Figure B-6 shows schematically the locations of the strain gauges placed on the 1990s design, which was also retrofitted onto a Budd Pioneer cab car. As the two figures show, the strain gauges were placed similarly on both the 1990s and SOA end frames to compare the way the load transfers through the end frame back into the rest of the vehicle.

Figure B-7 shows a photograph with the locations of strain gauges used on the 1990s end frame design. Two sets of strain gauges were used, and they are displayed in different colors in the photograph. All strain gauges shown were used for a series of quasistatic tests conducted to verify compliance of the end frame designs and supporting structure against the design requirements discussed in [4]. Only gauges shown by rectangles in the photograph were used for the dynamics impact test.

SOA End Frame
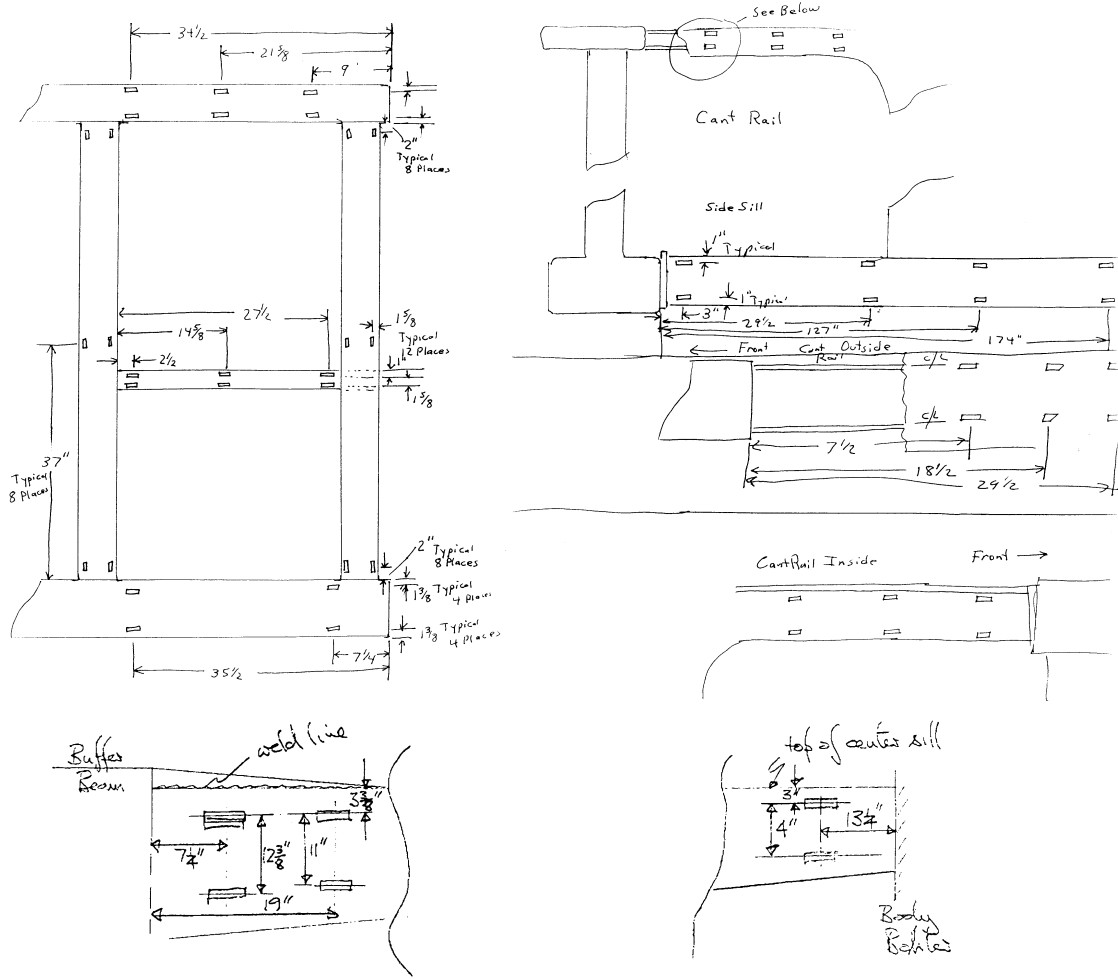
Figure B-5. Schematic of Strain Gauge Placement on SOA End Frame Design

Circa 1990s Design
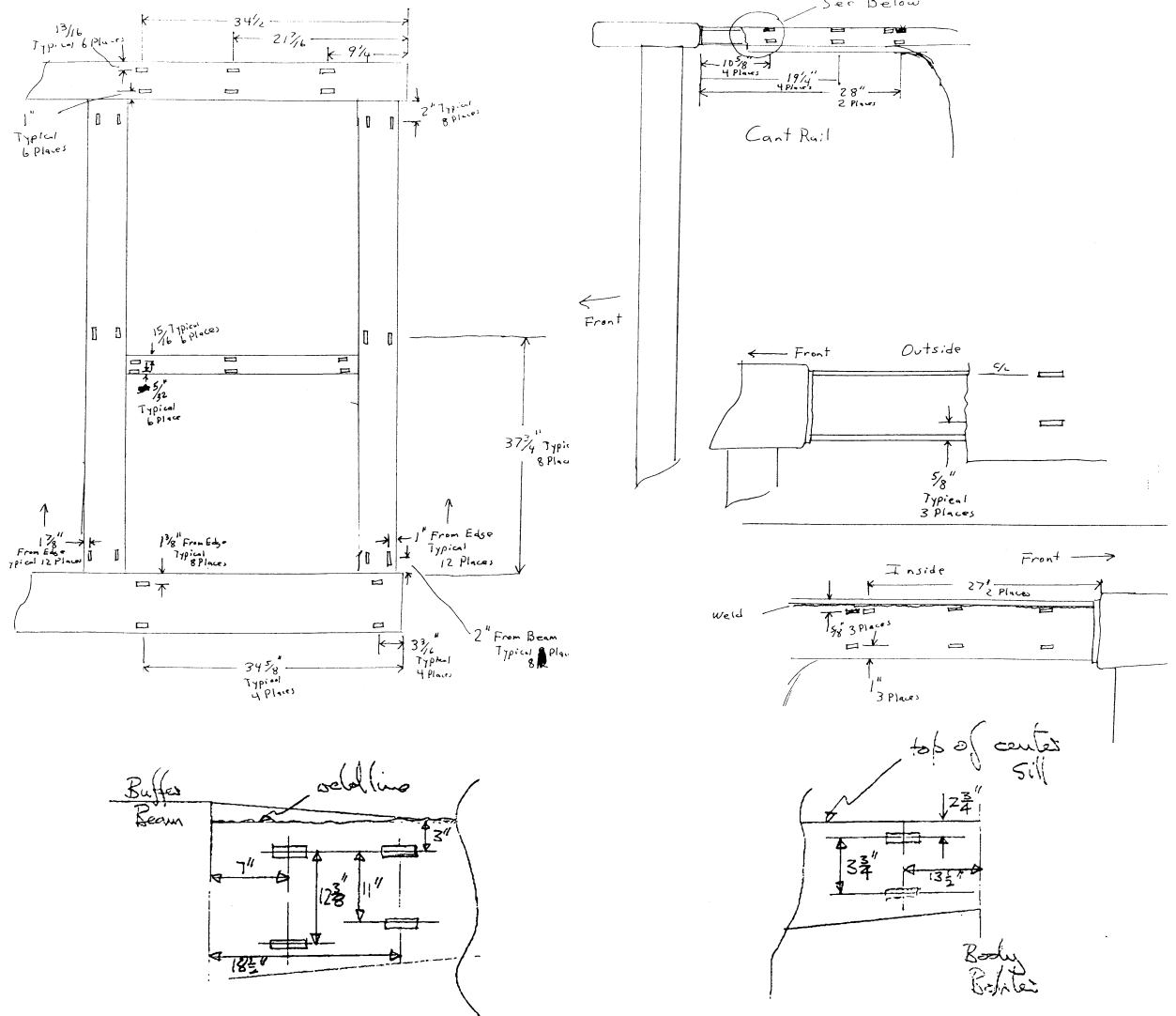
Figure B-6. Schematic of Strain Gauge Placement on 1990s End Frame Design

Figure B-7. Strain Gauges on 1990s End Frame Design

Eight high-speed cameras and four video cameras were used to record the impact from the following different angles: side-of-impact view of entire train, two side views focused on impact zone, head-on view, opposite side-of-impact angled view of front end, overhead view (camera located on a boom), and two onboard cameras (did not survive collisions). Figure B-8 shows placement of these cameras. The exterior high-speed cameras filmed at 300 frames per second, and the interior cameras filmed at 500 frames per second. Upon impact, contact switches, located on the coil and corner post, triggered flashes of light.
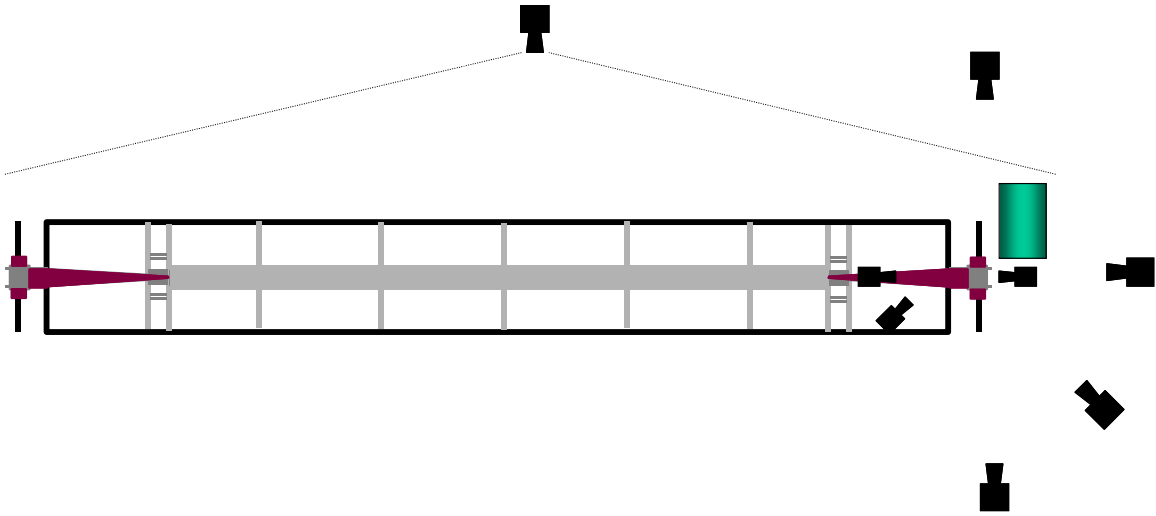
Figure B-8. Schematic Layout of High-Speed Camera Locations

Reflective 4-in diameter targets, placed on the end structure, facilitate photometric analysis of the film. The longitudinal and vertical coordinates of each target are identified with frame-by-frame grid analysis, and the speeds and location of the specific elements are then calculated.

References

1. American Public Transportation Association, Member Services Department, *Manual of Standards and Recommended Practices for Passenger Rail Equipment*, Issue of July 1, 1999.

2. U.S. Department of Transportation, Federal Railroad Administration, "49 CFR Part 216 et al., Passenger Equipment Safety Standards; Final Rule," *Federal Register*, May 12, 1999.

3. Penrose, R., *The Emperor's New Mind: Concerning Computers, Minds, and the Laws of Physics* (New York: Penguin Books, 1991).

4. Mayville, R., Stringfellow, R., and Martinez, E., "Development of Conventional Cab Car End Structure Designs For Full Scale Testing," U.S. Department of Transportation, to be published.

5. Martinez, E., Tyrell, D., and Zolock, J., "Rail-Car Impact Tests with Steel Coil: Car Crush," American Society of Mechanical Engineers, Paper No. JRC2003-1656, April 2003.

6. Jacobsen, K., Tyrell, D., and Perlman, A.B., "Rail-Car Impact Tests with Steel Coil: Collision Dynamics" American Society of Mechanical Engineers, Paper No. JRC2003-1655, April 2003.

7. National Transportation Safety Board, "Collision of Reading Company Commuter Train and Tractor-Semitrailer, Near Yardley Pennsylvania, June 5, 1975," RAR-76-4, March 3, 1976.

8. National Transportation Safety Board, "Collision of Northern Indiana Commuter Transportation District Train 102 with a Tractor-Trailer Portage, Indiana June 18, 1998,"RAR-99-03, July 26, 1999.

9. White, J.H., Jr., *The American Railroad Passenger Car* (Baltimore: The Johns Hopkins University Press, 1978).

10. *ABAQUS/Explicit Users Manual*, Version 5.8, 1998, Hibbitt, Karlsson and Sorenson, Inc.

11. *ADAMS, Version 12.0.0*, Mechanical Dynamics, Inc. Ann Arbor, Michigan.

12. Bao, Y., and Wierzbicki, T., "Determination of Fracture Locus for the 2024T351 Aluminum," Impact and Crashworthiness Laboratory, Report No. 81, May 2002.

13. Bao, Y., and Wierzbicki, T., "Comparative Study of Fracture Criteria: Part II–Finite Element Analysis," Impact and Crashworthiness Laboratory, Report No. 67, November 2001.

14. Tyrell, D., Severson, K., Marquis, B., and Perlman, A.B., "Simulation of an Oblique Collision of a Locomotive and an Intermodal Container," *Crashworthiness, Occupant Protection and Biomechanics in Transportation Systems*, American Society of Mechanical Engineers, AMD Vol. 237/BED Vol. 45, 1999.

15. Tyrell, D., Severson, K., and Perlman, A.B., "Single Passenger Rail Car Impact Test Volume I: Overview and Selected Results," U.S. Department of Transportation, DOT/FRA/ORD-00/02.1, March 2000.

16. Tyrell, D., Severson, K., and Perlman, A.B., "Passenger Rail Two-Car Impact Test Volume I: Overview and Selected Results," U.S. Department of Transportation, DOT/FRA/ORD-01/22.I, January 2002.

17. Society of Automotive Engineers, "Surface Vehicle Recommended Practices–Instrumentation for Impact Test," SAE J211-1, March 1995.

18. Severson, K., Tyrell, D., and Perlman, A.B., "Rail Passenger Equipment Collision Tests: Analysis of Structural Measurements," Rail Transportation, American Society of Mechanical Engineers, RTD-Vol. 19, 2000.

19. Blader, F.B., 1989, "A Review of Literature and Methodologies in the Study of Derailments Caused by Excessive Forces at the Wheel/Rail Interface," Association of American Railroads, Research and Test Department, Report No. R-717.

20. Lee, H., Plank, G., Weinstock, H., and Coltman, M., *Methodology for the Calibration of the Data Acquisition with a Six Degree-of-Freedom Acceleration Measurement Device*, DOT-TSC-NHTSA-88-03, U.S. Department of Transportation, Transportation Systems Center, 1989.

Acronyms

AAR	Association of American Railroads
APTA	American Public Transportation Association
AT	anti-telescoping
C&S	Construction and Structural
CD	collision dynamics
CEO	Corporate Executive Officer
CFC	Collision Frequency Class
FE	finite element
FRA	Federal Railroad Administration
PRESS	Passenger Rail Equipment Safety Standards
SAE	Society of Automotive Engineers
SOA	state-of-the-art
TTC	Transportation Technology Center